UNIVERSITY OF NOVA GORICA
SCHOOL OF SCIENCE

FLARES FROM THE CENTERS OF GALAXIES IN GAIA AND OGLE SURVEYS

MASTER'S THESIS

Nada Ihanec

Mentors: prof. dr. Andreja Gomboc
dr. hab. Łukasz Wyrzykowski

Nova Gorica, 2018

Acknowledgments

Foremost, I would like to express my sincere gratitude to my advisors Andreja Gomboc and Łukasz Wyrzykowski for all of their support, encouragement, effort and time they have dedicated to the realization of this thesis.

A great amount of gratitude also goes to Mariusz Gromadzki from Astronomical Observatory, University of Warsaw who was a part of our group for follow-up observations.

Finally, I must express my very profound gratitude to my family and friends for providing me with support and continuous encouragement throughout all my years of study and through the process of researching and writing this thesis.

Povzetek

Sodobni vsenebni in široko-kotni pregledi neba s sateliti in teleskopi na Zemlji dnevno opazujejo velike dele neba in vsakodnevno odkrivajo nove astrofizikalne vire.

V tem delu sem analizirala podatke z Esinega satelita Gaia in poljskega teleskopa OGLE. Osredotočila sem se na tranzientne dogodke, ki se nahajajo v središčih galaksij, da bi odkrila tako imenovana plimska raztrganja zvezd. Ta se zgodijo, ko se zvezda približa supermasivni črni luknji, kakršne se nahajajo v središčih večine galaksij. Plimske sile črne luknje so ob takih srečanjih močnejše od lastne gravitacije zvezde in jo raztrgajo.

Cilj mojega dela je bil iskanje plimskih raztrganj zvezd in izločitev drugih "nepravih" dogodkov, kot so na primer supernove. Dnevno sem analizirala podatke s satelita Gaia in teleskopa OGLE ter iskala tranzientne izvore v bližini središč galaksij. V primeru takšne detekcije sem sprožila nadaljna spektroskopska opazovanja, da bi pomagala klasificirati zaznane objekte.

V okviru mojega dela sem analizirala spektre, dobljene z največjimi teleskopi na svetu, SALT in VLT. Na dobljene spektre sem prilagajala spektre znanih vrst tranzientnih izvorov, prepoznavala njihove značilne lastnosti, določala kozmološki rdeči premik dobljenih spektrov in podobno.

Ključne besede: Gaia, OGLE, tranzienti, supernove, črne luknje, plimsko raztrganje zvezd
PACS: 04.70.Dy, 04.50.Gh, 96.50.sd

Abstract

Modern wide-field-of-view and all-sky satellites (e.g. Gaia) and ground based surveys (e.g. OGLE) repeatedly cover a large part of the sky and are detecting new, transient astrophysical sources on daily basis. In this thesis I analyzed the data from Gaia and OGLE transient surveys, with special focus on transients located near the centres of galaxies to detect possible Tidal Disruption Events. These occur when a star gets too close to a Super-Massive Black Hole, which lurks in the centres of most galaxies, and gets disrupted due to the black hole's gravitational tidal forces.

The goal of my research was to detect possible Tidal Disruption Events and eliminate false candidates, such as supernovae. The work involved daily inspection of new alerts, identified with Gaia and OGLE Transient Detection System. I searched for potential transients in galactic nuclei and in case there was such a transient detected, follow-up spectroscopic observations were initiated in order to help classify the object.

During the course of my work I analyzed spectra obtained with the largest telescopes in the world (SALT, VLT) and performed the spectral template matching, recognition of spectral features related to known classes of transients, determination of redshift etc.

Keywords: transients, Gaia, OGLE, alerts, supernovae, black holes, tidal disruption events
PACS: 04.70.Dy, 04.50.Gh, 96.50.sd

Contents

1 Introduction

On the large scales our Universe appears to be static. On smaller scales most of the processes are long-term changes, unrecognized to a naked eye, lasting a few millions or billion years. There are however processes that undergo changes on timescales of a few seconds and last from seconds to days, weeks, or even several years. These so called *transients* are in general violent, deep sky events which are unpredictable and occur randomly regarding the direction in the sky. When such an event (in form of an explosion) takes place, the electromagnetic signature radiated as a result is transient in nature. It appears as a flash in the sky for a short period of time and then fades away.

So far numerous different types of transients have been discovered both in our own Galaxy and beyond. To name a few: Supernovae, Novae, Gamma-Ray Bursts, Gravitational microlensing events, Variable stars, Active Galactic Nuclei, Pulsars, Tidal Disruption Events, etc. These events are part of the broader topic of time domain astronomy, the study of how astronomical objects rapidly change with time. With the advent of robotically controlled telescopes and all-sky monitoring with high cadence the field of time domain astronomy has hugely evolved in the past decade.

Astronomical transients provide a unique opportunity for probing the fundamental physics at work in compact objects by studying their behavior in both the spectral and temporal domains. In my thesis I am interested in extragalactic transients especially Tidal disruption Events, which appear in nucleus of galaxies, with the aim of further understanding of the environment in which they occur. In the following subsections I will present types of transients which were relevant in my search.

1.1 Supernovae

Supernova (SN) is an astronomical event which occurs towards the end of life of massive stars and in which the energetic destruction is marked by a final explosion. At the time of the explosion, a huge amount of energy is emitted and can be seen as a sudden appearance of a new bright star-like object, which then slowly fades below the detection limit over several months to a few years. SNe can briefly outshine the entire host galaxies and are, next to neutron stars mergers, one of the sources of heavy elements in the universe. They expel most if not all of the material from a primary star with velocity, $10000\frac{\mathrm{km}}{\mathrm{s}} \sim (0.003\mathrm{c})$ in the form of shock waves through interstellar space[1]. In doing so a SN produces heavier elements (heavier than Iron) and expands a shell of gas, elements and dust which is observed as supernova remnant. The expanding shock can also trigger the formation of new stars and is believed to be a primary source for cosmic rays.

For now, we can in general distinguish between two basic mechanisms for creating supernovae ergo two types of different circumstances, which lead to a state of dynamic instability. One is a collapse of the iron core of massive star;

Core-colapse Supernovae, and the other is the collapse of a white dwarf which has reached Chandersekhar limiting mass; *Thermonuclear Supernovae* .

Supernovae types and subtypes are defined according to observational and photometric properties.

1.1.1 Thermonuclear Supernovae

After a star with mass up to $\sim 8M_{\odot}$ finishes fusing hydrogen into helium in core, the core gets heavier and contracts. The core becomes iso-thermal, with no nuclear reactions in it. Because of the temperature increase, hydrogen starts burning in a shell surrounding it and gradually He-core gets more and more mass. When it reaches maximum mass it contracts further and the core temperature rises enough for the helium to fuse into carbon. Surrounding the helium burning core is a shell of burning hydrogen. When all the helium in the core gets fused into carbon, a star succumbs to gravity again. If the core temperatures are not high enough to ignite carbon this causes a release of energy that makes the envelope of the star expand. The star in this stages is not stable and starts loosing its envelope as a Planetary Nebula leaving the core of the primary star as a White Dwarf (WD). They are very dense stars. Their size is comparable to the size of the planets such as Earth but their mass is much larger, with the Chandrasekhar limit of around $1.4\mathrm{M}_{\odot}$. Above this mass, electron pressure can no longer support the star and it collapses to an even denser state.

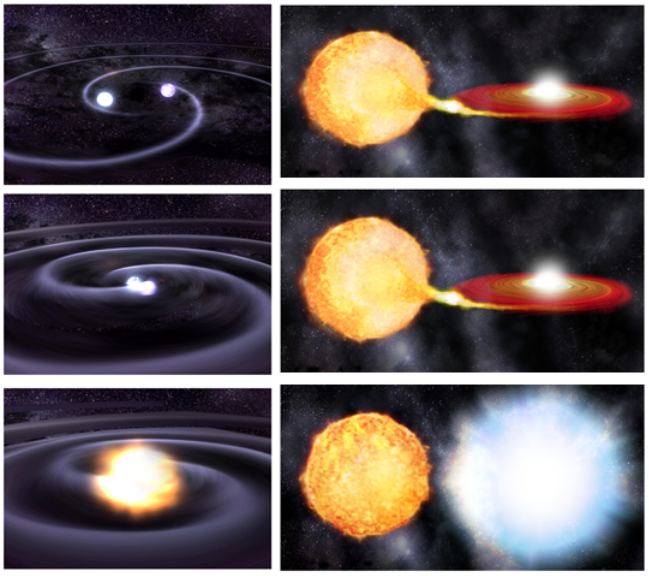

Figure 1.1: Two scenarios for progenitor of SN Ia. **Left** is double degenerate scenario and on the **right** single degenerate scenario. *(Images taken from Wikipedia Commons and Discover Magazine.)*

If a White Dwarf forms in a binary system with longer-lived main-sequence star and if her companion is close enough (and it fills its Roche lobe), the main-sequence star starts to transfer its matter onto the white dwarf, adding the material to the WD. When the WD reaches $1.4\mathrm{M}_{\odot}$, a nuclear chain reaction occurs, causing the WD to explode which is visible as *Supernova Type Ia* or in short *SN Ia*. Because this always happens approximately at the same mass, the absolute

magnitude is approximately the same. SN Ia are therefore the perfect Standard Candles, meaning we can determine their distance and use them for cosmological tests (measure the expansion rate of the Universe).

This so called *single degenerate scenario* was for many years believed to be the only possible way to produce SN Ia. There is however the second plausible explanation; *Double degenerate scenario*. (Figure 1.1).

In this case of Double degenerate scenario, there is a binary system of white dwarfs which merge due to the loss of angular momentum by emitting gravitational radiation. If the produced WD exceeds the Chandrasekhar mass it will explode as SN Ia.

SN Ia are the most commonly observed and also the most luminous of all types of SNe[12]. The spectrum observed in optical wavelengths has a particular shape (Figure 1.2). Fast rise to its peak, with wiggles and then it rapidly declines, with additional bump visible in red bands (I, J, K). The spectrum does not show any absorption lines of hydrogen or helium. The most prominent absorption line is Si II (6100Å) as well as lines from O, S, Ca and blends of Fe. Typically expansion velocities are around 11000km/s (deducted from Si II lines at the peak) and the typical peak magnitudes are $M = -19.1$ in B filter and $M = -18.67$ in R filter.

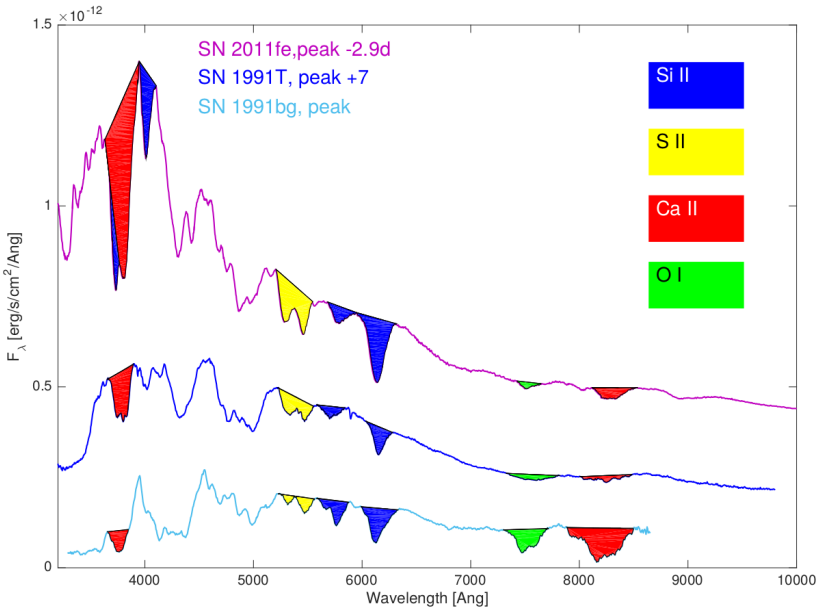

Figure 1.2: A spectrum of a normal SN Ia, obtained 2.9 days prior to peak B-band magnitude (top). The middle spectrum belongs to the SN 1991T, 7 days after the peak and the bottom one at the time of the peak. All the spectra are dominated by absorbtion lines, the major features are marked with colors[12].

.

1.1.2 Core-collapse Supernovae

Massive star ($> 8M_{\odot}$) will end its life as Core-collapse supernova (CC SN), leaving behind either neutron star or black hole. CC SN occur at the end of a massive star evolution. When the star leaves the main sequence (has no more hydrogen in its core), the contraction of the core rises the temperature so that

helium starts to burn. After the helium burning stage comes the carbon burning, neon burning, oxygen burning and silicon burning stages, each lasting a shorter period of time than the previous one. The end result is production of iron. Up until this stage, the enormous mass of the star has been supported against gravity by the energy released in fusion reactions. The formation of iron in the core concludes fusion processes and, with no energy to support it against gravity, the core begins to collapse in on itself.

During this final second, the collapse causes temperatures in the core to rise very fast, which releases very high-energy gamma rays. At this stage the core has already contracted beyond the point of electron degeneracy, and it continues contracting, in the end producing a Black Hole or a Neutron star.

Depending on initial mass and chemical composition, the stars collapse at different burning stages hence producing different types of CC SNe which can be characterize spectroscopically. There are two main classes - with and without hydrogen lines (type II and I respectively). Furthermore the subclasses are again determined with regards to presence/lack of certain spectral lines.

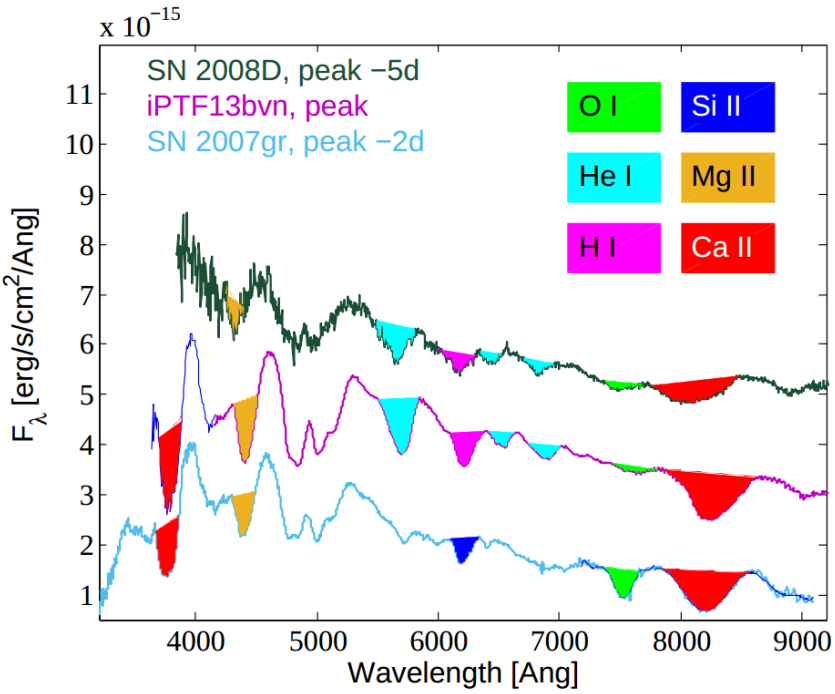

Figure 1.3: Spectra of three different SNe, first two (top and middle) considered to be regular SNe Ib and the third one (bottom) of typical SN Ic. Top spectrum was taken five days before peak magnitude, the middle at the time of the peak an bottom two days before peak. Major absorption features are marked with colors. As seen on the bottom spectrum, there are no HeI emission lines[12].

.

Types Ib and Ic don't show any hydrogen in their spectra. There are however some differences between them. SNe Ib show strong absorption of He I around the peak (see Figure 1.3), as for SNe Ic, they are defined by the lack of strong features of hydrogen and helium, see Figure 1.3 (the same as SN Ia, but the characteristic absorption features differ enough to distinguish between those two types). Another clear observational distinction between Type Ic SNe and SNe Ia

is the appearance of the late-time nebular spectra (Fig 1.4).

Furthermore subtype of Ib (SNe Ibn) show strong and relatively narrow He I emission lines in their early spectra. They can be quite luminous, typically peaking around -19 mag and quickly declining after maximum.

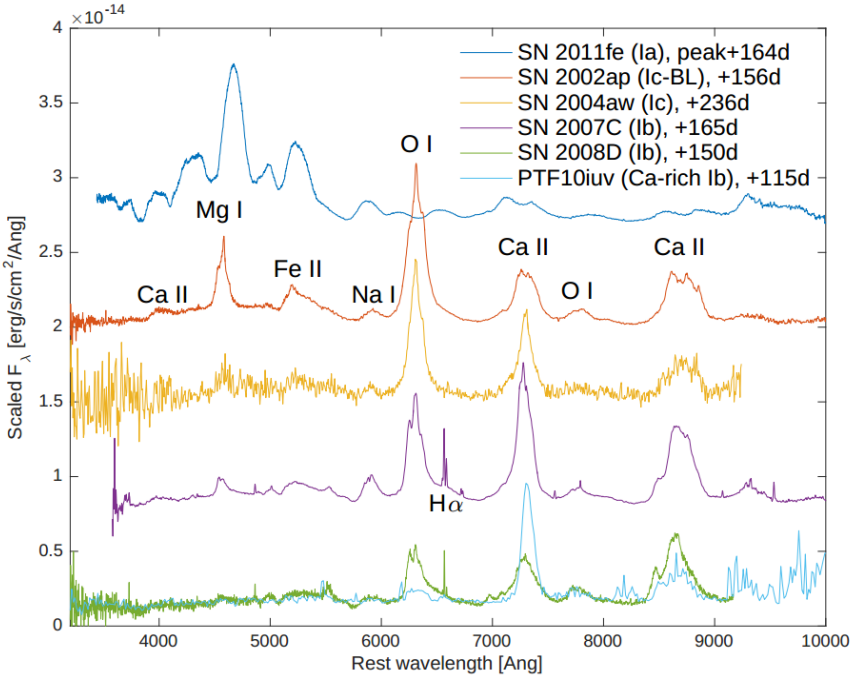

Figure 1.4: Nebular spectrum of Type I SNe. The nebular spectrum of regular SNe Ia shows strong blends of Fe-group elements in the blue (4000-5300Å), while spectra of SNe Ib and SNe Ic are dominated by strong emission of intermediate-mass elements such as O, Mg, and Ca. Ca-rich SNe Ib show strong Ca II emission and weak or absent OI[12].

.

The second class, type II SNe are known by strong absorption lines of hydrogen (mostly Balmer Hα) even few weeks after the explosion. Spectroscopically SNe II show a range of light curve shapes all with a mean peak absolute R-band magnitude of -17.14. SNe IIP have flat evolution in red light and show light curve plateau, SNe IIL show relatively rapid and linear declining light curves.

Type IIb initially resemble SN II and then evolve to resemble SN Ib and are relatively rare subclass ($5-10\%$ of SNe II [6]) but are still relatively well studied. The mean peak magnitudes are of -17.94 mag in R-filter. Their light curves show initial early bump and are similar to SNe Ib and Ic.

Another subtype of SN II are SNe IIn with a prominent narrow emission lines. They are known for their strong interactions with circumstellar medium (CSM) surrounding the progenitor. The spectrum have a slow evolution and are dominated by strong Balmer and He I emission lines without broad absorptions with a mean peak magnitude of -18.77 in R-filter. Balmer lines (in particular $H\alpha$) show well defined three component structure with broad ($FWHM \approx 15000$km/s), intermediate ($FWHM \approx 2200$km/s) and narrow ($FWHM < 700$km/s) components (Figure 1.6)[13].

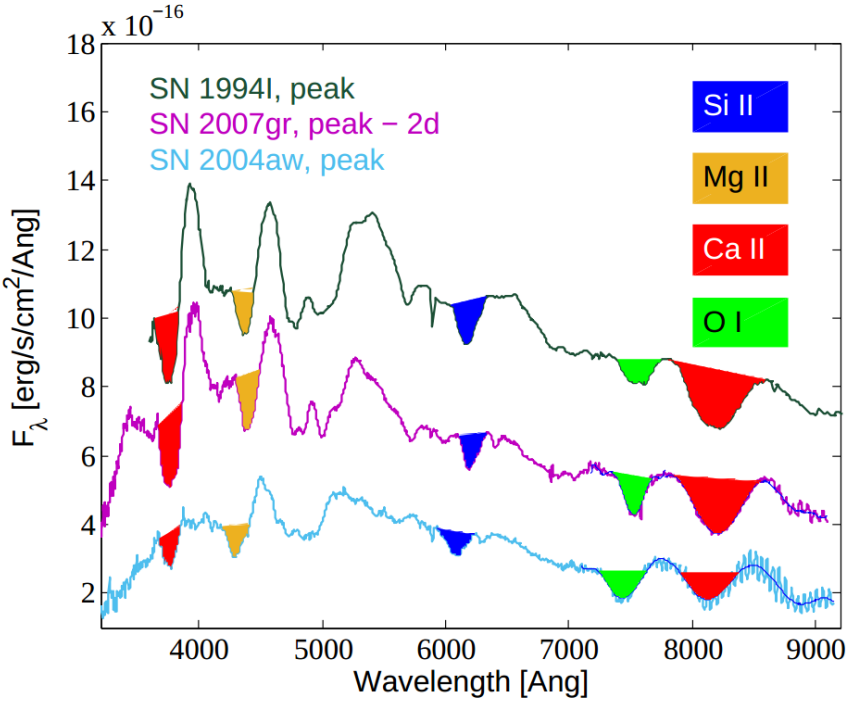

Figure 1.5: Spectra of events considered to be regular SNe Ic. Major absorption features by intermediate-mass elements are marked, while the spectral shape in the blue part is dominated by multiple absorption features from iron-group elements. The bottom spectrum shows higher velocities and more line blending compared to the other two[12].

.

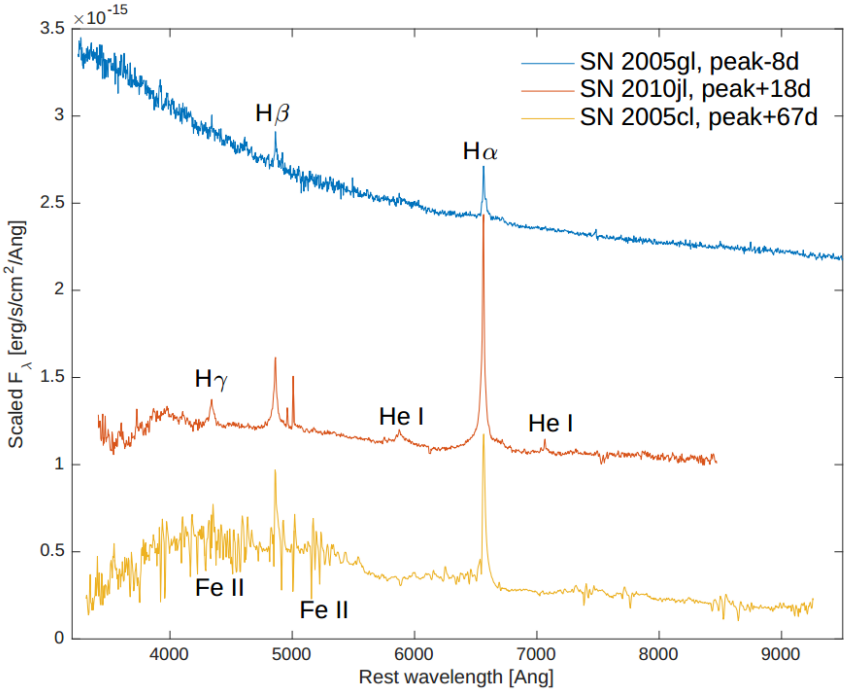

Figure 1.6: Spectra of SNe IIn at pre-peak, post-peak and in later phases (top, middle and bottom respectively) with clear Balmer emission lines and in later stages numerous narrow lines of Fe II. The three spectra represent diverse nature of this class of events[12].

.

1.2 Events evolving in the vicinity of black holes

One of the predictions of general relativity states that gravitational field which is present due to a compact, massive object can be so intense that nothing can escape its gravitational pull. John Archibald Wheeler first named such objects as black holes (BHs). Depending on their mass black holes are categorized in four main categories: supermassive black holes ($M_{SMBH} > 10^5 \mathrm{M}_\odot$), intermediate mass black holes ($M_{IBH} \approx 100 - 10^5 \mathrm{M}_\odot$), stellar mass black holes ($M_{BH} < 100 \mathrm{M}_\odot$) and miniature black holes ($M_{BH} < \mathrm{M}_\odot$). The size of a BH is determined with the radius of its event horizon (a boundary in spacetime through which matter and light can only pass towards BH), or Schwarzschild radius (R_s):

$$R_s = \frac{2MG}{c^2} \approx 3\frac{M}{M_\odot}\mathrm{km}. \tag{1.1}$$

Because no light can escape from a BH, it is impossible to detect it directly. The indirect methods for studying BHs depend on their mass. Stellar BHs can be studied if a BH is in a binary system with a star. Properties of a BH can be determined through analysis of the motion of the companion. Another possibility is to study radiation which is produced by gas stripped from a companion star. In rare cases, stellar BHs can be studied via microlensing events.
Massive Black Holes ($M_{MBH} > 100 \mathrm{M}_\odot$) can also be studied with radiation from the gas that can accrete around MBH. In this respect they can be classified in two categories, accreting or active BHs and quiescent or dormant BHs. In first case gas is more abundant and falls to the BH at higher rates, in the second only small amounts of material is falling towards the BH.
SMBH can be found in the centre of most massive galaxies including our own. The properties of the black hole in our Galactic centre were determined by studying the motion of the stars in the centre. However this can only be done in our galaxy because all others are too far away, to be observed in detail with current telescopes.
Existence of IMBHs is yet to be proven observationally beyond doubt.

It is currently believed that the galaxies today are most likely a product of mergers of smaller galaxies. After the merger of two small galaxies, their central black holes (potentially also the elusive intermediate-mass black holes, IMBHs) will merge as well so the mergers may play an important role in building SMBHs. The other possibility is also fueling the IMBH with matter in the form of gas (as in a case of Active Galactic Nuclei - AGNs) or with stars which could happen in a case of tidal disruption events (see Figure 1.7).

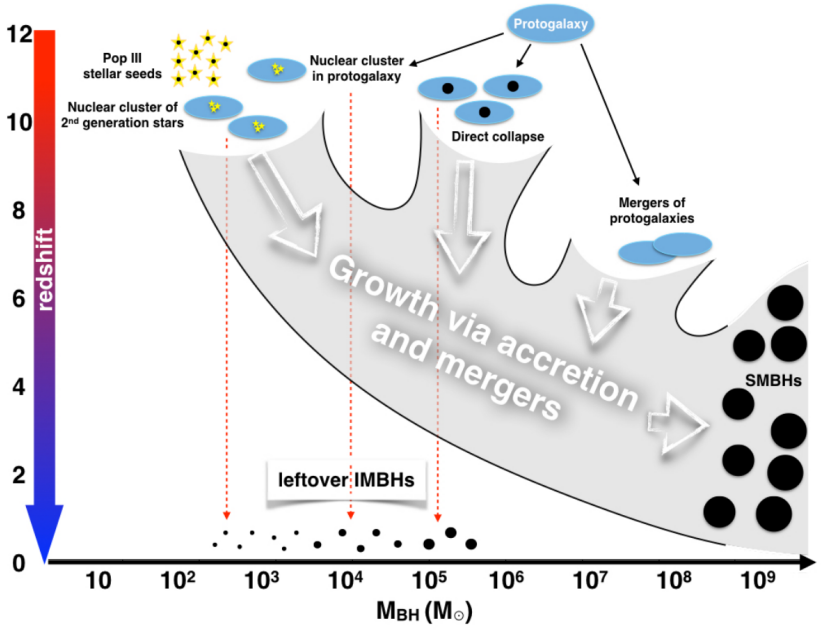

Figure 1.7: Formation scenarios for IMBHs. [7]

1.2.1 Active Galactic Nuclei

In the centre of most galaxies, there lurks a supermassive black hole. The majority of them are quiescent but around 10% of them have active, very bright nuclei and were therefore given a name active galaxies or Active Galactic Nuclei (AGN).

Active galaxies are galaxies in which a significant fraction of the electromagnetic energy output is not contributed by stars or interstellar gas. They emit radiation that does not follow the typical black-body spectra of stars but is non-thermal. They emit more energy at shorter wavelengths (ergo higher energies) than objects which radiate as black-bodies. Majority of this emission comes from the galactic nuclei. The main features of an AGN are: compact ($\sim$ 3pc) and extremely luminous centre, two beams (jets) coming from the nucleus in opposite directions, strong non-thermal radio or X-ray emission, spectrum with strong emission lines, strong ultraviolet emission from a compact region in the centre, variability over the whole spectrum on short timescales and strongly Doppler broadened emission lines. Jets are however not observed in all the AGNs.

The key process in the physics of AGN is accumulation of gas into central black hole under the influence of gravity, producing an accreting disk. The generally accepted model for AGN is that there is an accretion disk of in-falling material surrounding the black hole. In this disc gravitational energy of the matter is transformed into heat - therefore disc is very hot and emits radiation, which is responsible for huge luminosities of AGN.

AGNs show variability in their luminosity on timescales of $\Delta t \approx 10^4$s[24]. Variability can be seen only if the area in which the variability occurs is smaller than the distance the light travels in that time, i.e. $c\Delta t$. This means that the size of accreting disk is smaller than:

$$R < c\Delta t \approx 3 * 10^8 \frac{\mathrm{m}}{\mathrm{s}} 10^4 \mathrm{s} \approx 3 * 10^{12} \mathrm{m} \approx 10^{-4} \mathrm{pc} \tag{1.2}$$

The average luminosity for an AGN is of the order of 10^{45}erg [1]. For such small area to emit so much energy the only plausible explanation is a black hole.If we compare this size to the Schwarzschild radius we find that the mass of the black hole of this size would be:

$$M = \frac{Rc^2}{2G} = \frac{10^{12}\mathrm{m} * (3 * 10^8 \frac{\mathrm{m}}{\mathrm{s}})^2}{2 * 6.67 * 10^{-11} \frac{\mathrm{m}^3}{\mathrm{kgs}^2}} = 6.7 * 10^{38}\mathrm{kg} \approx 10^8 \mathrm{M}_\odot \tag{1.3}$$

For any accreting object, there is a maximum luminosity beyond which radiation pressure will overcome gravity, and material outside the object will be pushed away from it rather than falling inwards. This limiting luminosity, *Eddington luminosity* is

$$L_{Edd} = \frac{4\pi G M m_p c}{\sigma_T} \sim 3 \cdot 10^4 \frac{M}{M_\odot} L_\odot \tag{1.4}$$

Here σ_T is the Thomson scattering cross-section, M is the mass of accreting object, m_p is the mass of the proton, $\mathrm{M}_\odot$ is the Solar mass and $\mathrm{L}_\odot$ is the Solar luminosity.

If we use typical AGN luminosity and put it in Equation 1.4 we can calculate mass needed for this luminosity:

$$M = \frac{L}{3 \cdot 10^4 L_\odot} M_\odot \approx \frac{10^{38}\mathrm{W}}{4 \cdot 10^{26}\mathrm{W} \cdot 3 \cdot 10^4} M_\odot \sim 10^7 M_\odot \tag{1.5}$$

from this we can see that it is not enough to take a small, stellar mass black hole, but that we need a massive one to sustain this luminosity.

This expression was obtained under the assumptions, that we have pure, ionized hydrogen gas and spherically symmetric inflow of material.

Typically, AGNs are divided in two categories, *radio-quiet* and *radio-loud*, depending on the presence of radio emission in both accretion disc and jets. Furthermore, depending on the position of our line of sight with respect to an AGN, we distinguish different types of active galaxies shown in Figure 1.8, all part of Unified model of AGNs.

Based on their spectra, AGNs can be easily distinguished from quiescent galaxies. They have very strong emission lins (both narrow and broad). For example Seyfert galaxies type I show both broad and narrow lines while type II show only narrow lines. Those lines come from different regions of AGN as can be seen in Figure 1.8. Broad lines are Doppler-broadened and in the narrow line region mostly the forbidden lines are formed. Figure 1.9 shows spectra of different types of AGNs and table 1.1 some features of different types of AGNs.

[1] 1 *erg* is equal to 10^{-1}J

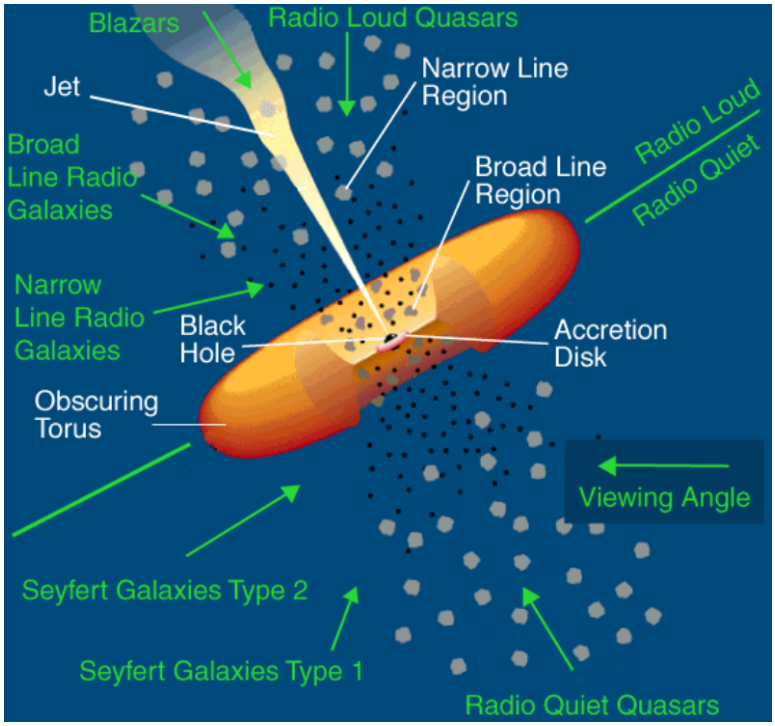

Figure 1.8: Unified model of AGNs. [24]

Type	Emission lines	Radio emission	jets	L [erg s^{-1}]
Blazar	weak BL	strong	yes	10^{45}-10^{49}
Radio-loud quasar	BL	strong	yes	10^{45}-10^{49}
Broad -line radio galaxy	BL	strong	yes	10^{45}-10^{49}
Narrow-line radio galaxy	NL	strong	yes	10^{45}-10^{49}
Seyfert 1	BL, NL	no	no	10^{43}-10^{45}
Seyfert 2	NL	no	no	10^{43}-10^{45}
Radio-quiet quasar	NL	no	no	10^{45}-10^{49}

Table 1.1: Main properties of different types of AGNs. BL stands for broad lines in spectrum and NL for narrow lines.

1.2.2 Tidal Disruption Events

Tidal Disruption Event (TDE) is the phenomenon observed when a star gets too close to a Supermassive Black Hole (SMBH) in a centre of a galaxy and gets disrupted by its tidal forces [2].

TDE occurs when a star (with radius R_* and mass M_*), which is moving on an eccentric orbit under the influence of the SMBH (of mass M_{SMBH}), approaches SMBH. If the distance of the closest approach, the pericentre distance R_P, is smaller than radius of the tidal sphere with R_T

$$R_T = R_* \left(\frac{M_{SMBH}}{M_*} \right)^{1/3}, \tag{1.6}$$

the tidal forces of the black hole overcomes self-gravity of the star and the tidal field totally or just partially disrupts the star (depending on the structure of the

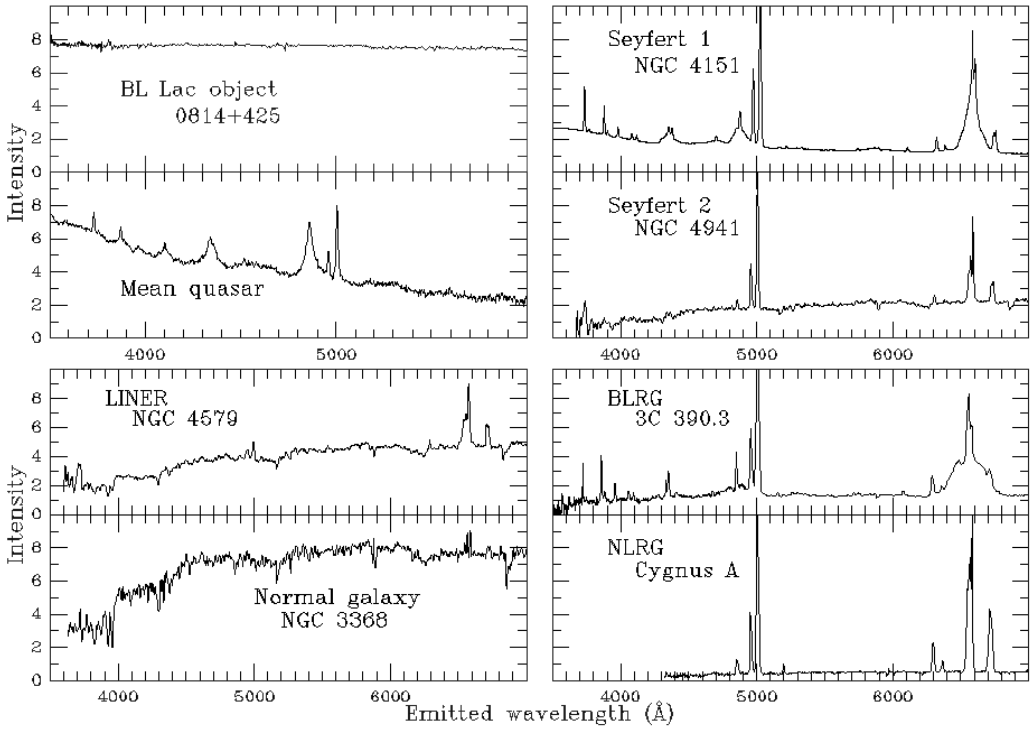

Figure 1.9: Typical spectra for different types of AGNs.

star). Part of stellar debris from disruption will fall back onto the BH and form a viscous accretion disc and in doing so, produce a luminous flare [4].

The minimal energy required for the tidal disruption of a star has to be at least equal to the star's self binding energy (of the order of $\frac{G(M_*)^2}{R_*}$). When the star approaches the pericentre, different areas of the star feel different gravitational pull. This causes a sizeble spread in specific orbital energy ϵ within the star. The parts closest to the black hole have a negative specific binding energy, and the parts furthest from BH have positive specific binding energy. Because of the different parts of the star being at different distances to the BH, the spread around the mean energy is approximately $\frac{R_*}{R_P} = (\frac{M_{SMBH}}{M_*})^{1/3}$. The specific energy spread can be therefore estimated as [34]

$$\Delta\epsilon = \mp\frac{GM_*}{R_*}\left(\frac{M_{SMBH}}{M_*}\right)^{1/3} = \mp\frac{GM_{SMBH}}{R_*^2}R_P \tag{1.7}$$

The stellar debris with specific orbital energy $\epsilon<0$ remains bound to the black hole, eventually creating accretion disc just outside of the black hole's event horizon, the rest, with $\epsilon>0$, escapes the gravitational pull of the black hole. The gas in the accretion disk is heavily heated as it falls to the black hole, thus producing a flare. The accretion disc is consumed by the black hole on time scales from months to years. The development of the event is illustrated in Figure 1.10.

The disruption will occur and will be visible if $R_S<R_P<R_T$. The limiting mass of the black hole (when $R_T=R_S$) is therefore

$$M_{BH} = \left(\frac{R_* c^2}{2M_*^{1/3}G}\right)^{3/2}. \tag{1.8}$$

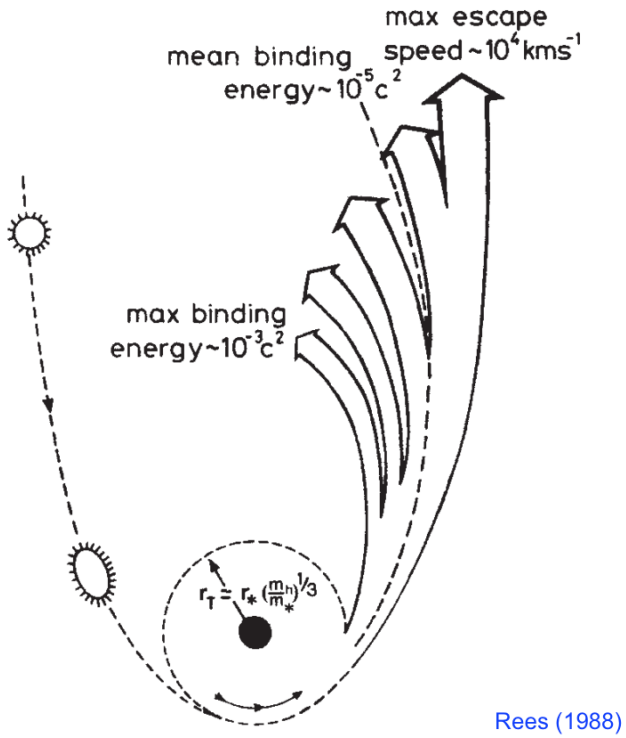

Figure 1.10: The star is aproaching (on the left) the SMBH on parabolic orbit. During a fly-by past the SMBH at the distance of R_T it disrupted partially. Part of the debris gets pulled back and accreates around SMBH, while the rest escapes [2].

For a Sun-like stars the limiting mass is $10^8 \mathrm{M}_\odot$. For a Sun-like stars, TDEs will most commonly occurr in galaxies with BH masses $10^6 - 10^8 M_\odot$. Figure 1.11 shows tidal and Schwarzschild radius for different masses of BH for a Sun-like star.

Most theoretical studies predict TDE rate of the order of $10^{-4}\mathrm{yr}^{-1}\mathrm{gal}^{-1}$ however observations estimate rate of the order of $10^{-5}\mathrm{yr}^{-1}\mathrm{gal}^{-1}$, for $M_{BH} \leq 10^{7.5}\mathrm{M}_\odot$ [29]. Therefore only once in a 10000 to 100000 years a star will be disrupted in a galaxy. Because of the small rate, large field of view or all-sky surveys are necessary for detection and study of TDEs.

The majority of the observed TDEs so fare were detected in the rare type of galaxies E+A [5]. Those are elliptical galaxies with a huge population of A type stars which indicates the age of the galaxy to be maximally 1 Gyr and the presence of recent star formation which probably occurred because of the merger between two galaxies.

TDEs are detected mostly in optical light, though some of them were also detected in UV, gamma and X-rays. They are one of the most luminous events, with absolute magnitude -20 up to -23 mag and optical luminosities, typically between 10^{43} and 10^{44} erg/s. Their spectrum can be well fitted by a black-body spectrum with temperatures from $10^4 - 10^5 K$.

The spectrum of a TDE is characterized by a very blue, thermal shape with the most prominent broad HeII line and broad Balmer lines. (Figure 1.12). The HeII broad emission line is the best indicator for distinguishing TDEs from other

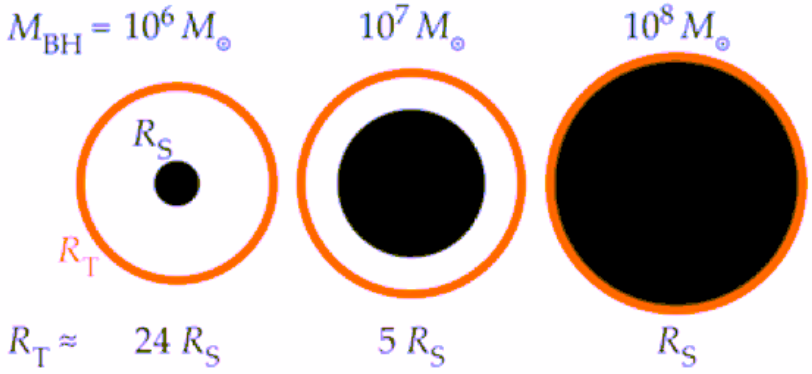

Figure 1.11: Tidal radius (R_T, orange circle) and Schwarschild radius (R_S,black circle) for a Sun-like star and three different BH masses. Adapted from [30].

transients (mostly supernovae) as it indicates high temperatures and huge amount of accreted material with different velocities circling BH.

The light curve is generally well fitted with $t^{-5/3}$. Theoretically, the initial evolution shows a relatively gentle rise with time. At early times, emission in optical bands is dominated by the outflow component. After the peak luminosity, around a month after disruption, the light curve decreases as $t^{-2.6}$ until contribution from the disk takes over. The shape of a lightcurve is shown in Figure 1.12.

TDEs were first predicted in 1980s[2], and the first TDE candidate found in an optical surveys was discovered by van Velzen et al. (2011). Since then, the number of TDE discovered in optical surveys has rapidly increased, with about 80 candidates[2], however, due to the lack of detailed follow up observations, only a few of them were confirmed to be TDEs.

TDEs offer a unique opportunity to study the mass of SMBHs in quiescent galaxies, the stellar populations and dynamics in galactic nuclei, the physics of black hole accretion under extreme conditions including the potential to detect relativistic effects near the SMBH, and the physics of radio jet formation and evolution. AGNs host SMBHs that are supplied by steady streams of gas for hundreds or even thousands of years, TDEs on the other hand offer a unique opportunity to study a single SMBH under feeding conditions that change over timescales of days or months. TDEs offer an opportunity to study the evolution of their accretion disks for a wide range of mass accretion rates and feeding timescales, by testing different theoretical models and comparing them with observational data.

[2]The open TDE catalog can be found at https://tde.space/

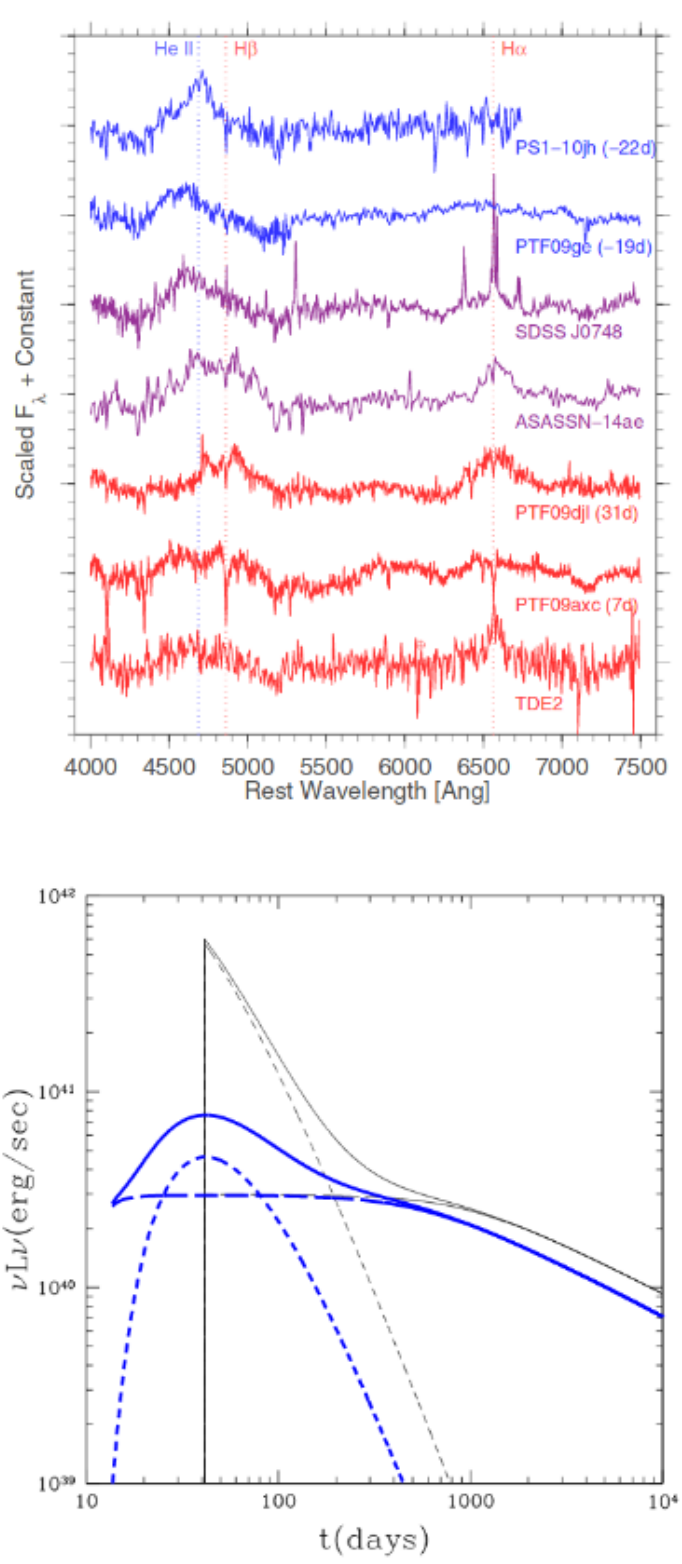

Figure 1.12: Top: Spectra of seven good candidates for TDE. Broad HeII and Hα emission lines can be seen. [5] Bottom: Theoretical lightcurve for a TDE in G-band, for a Solar-type star, R_T/R_P=1, a BH mass 10^6 $M_\odot$. The solid black line represents a total lightcurve, the short-dashed line indicates the wind component and the long-dashed line the disc component. After approximatelly a year, the disc dominates the emission. Adapted from [30].

2 Surveys and follow-up

Since the rate of nuclear transients is low (for TDEs $10^{-4} - 10^{-5}$ per galaxy per year [29]), wide field of view and all-sky surveys are crucial for their detection. The detection itself is however not enough. For further studying and understanding these events, follow-up observations are necessary.

In my work, I was trying to find transients in the nuclei of galaxies with the aim of identifying those which could be tidal disruption events. The candidates provided for my research were observed by two different surveys: Gaia Science Alerts project using Gaia satellite data, and OGLE-IV Transient Detection System on OGLE telescope.

2.1 Gaia

Gaia (Figure 2.1) is European Space Agency (ESA's) space astrometric mission, launched on 19 December 2013. The satellite arrived to it's final destination, L2 point of the Sun-Earth system, about a month after the launch and is fully operational since July 2014. Its primary goal is to observe more than one billion bright objects in the Milky Way and provide high-precision astrometric measurements, meaning position, parallax and proper motion of stars, down to magnitude V=20 mag resulting in the most precise three-dimensional map of our Galaxy. In five years of operations the entire sky will be scanned on average of 70 times, depending on necessity and significance of the region up to 200 times (Figure 2.2). Gaia is also capable of detecting variability with millimag precision which makes it also a good all-sky transient survey.

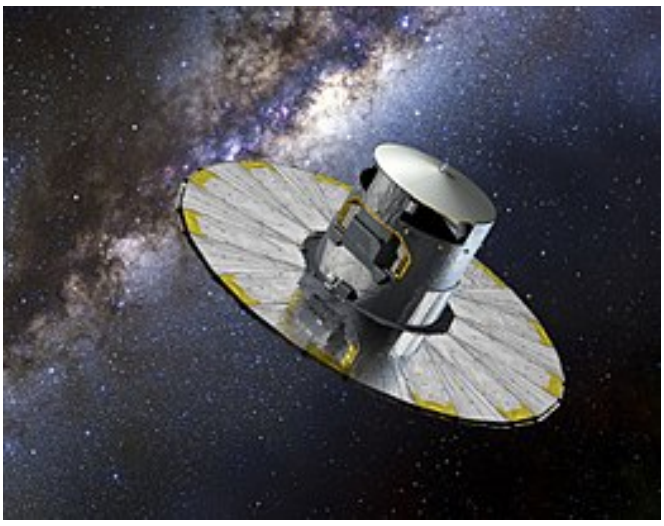

Figure 2.1: Gaia satelite with the Milky Way - artistic impression.

Gaia satellite is slowly rotating at a constant angular rate of 1° per minute around axis, and therefore completes one rotation in 6 hours. Additionally the

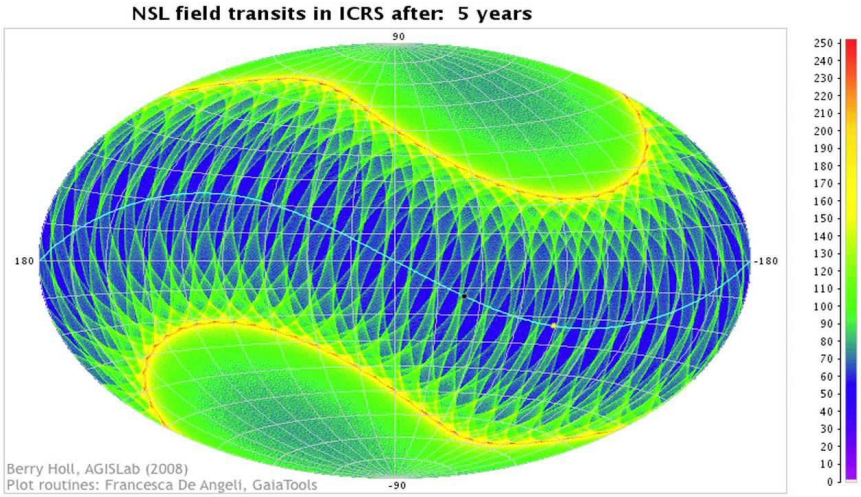

Figure 2.2: Sky coverage of Gaia in 5 years.

spin axis precesses with period of 63 days with fixed angle 45° from the Sun, allowing repeated full sky coverage. The entire sky is therefore observed after 183 days. The spacecraft has two rectangular mirrors (telescopes), with fixed separating angle 106.5° with the field of view of 0.7° x 0.7° each (Figure 2.3). The result is that the objects are scanned along the great circle perpendicular to the spin axis and that objects transit the second field of view with a delay of 106.5 minutes compared to the first field, producing the coverage shown in Figure 2.2.

From each telescope, the light from an object enters through aperture striking the primary mirror. The light is then reflected and bounced by a series of mirrors along a 35 m long focal length at the end of which lies the beam combiner which combines the two light paths and is imaged onto single focal plane, containing 106 CCDs (approximately 1 Gigapixel camera). The focal plane serves five main functions (see Figure 2.4):

- Covering $2+2$ CCDs are basic angle monitor and wave-front sensor (one for each mirror). A five degrees of freedom mechanism is implemented behind the secondary mirrors of the two telescopes for re-aligning the telescopes in orbit to cancel errors due to mirror micro-settings and gravity release.
- The sky Mapper (SM), containing 7 CCDs per telescope. They autonomously detect objects down to 20 mag.
- The main Astrometric Field (AF) with 9 rows of CCDs, in total of 62 CCDs. For angular-position measurements, providing position (two angles), proper motion (two time derivatives of position), and distance (parallax) of all detected objects.
- The red and blue photometers (RP and BP respectively). They are fused silica prisms, dispersing all the light entering the field of view. The spectral resolution is a function of wavelength and varies in BP from 4 to 32 nm pixel^{-1} covering the wavelength range 330-680 nm. In RP, the wavelength range is 640–1050 nm, with a resolution of 7 to 15 nm pixel^{-1}.
- The radial velocity spectrometer (RVS), covering 3×4 CCDs. They collect high resolution spectra of objects brighter than 17 mag. The resolution for

bright stars up to $V \sim 11$ is $R \sim 11500$ and for faint stars up to $V \sim 17$ is $R \sim 5000$.

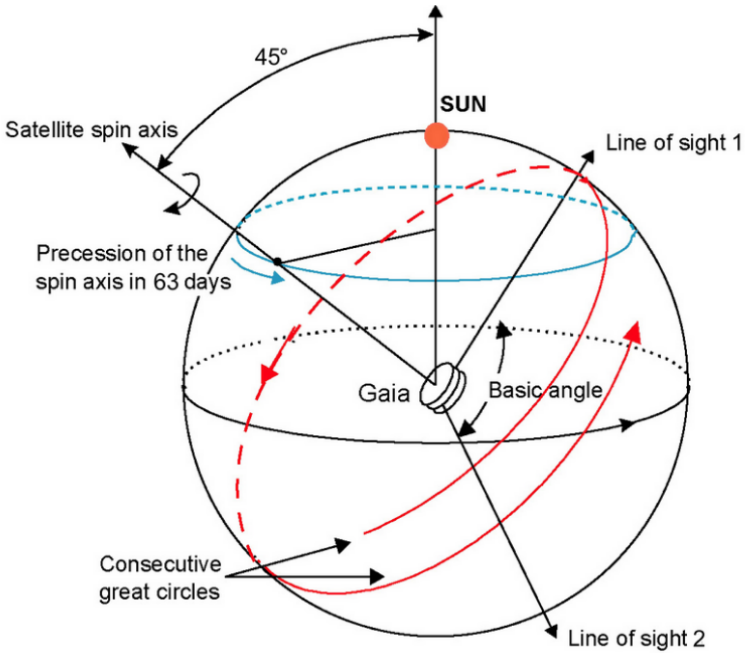

Figure 2.3: The spacecraft rotation axis makes an angle of 45° with the Sun direction, making it the optimal point between astrometry requirements, and implementation constraints - such as payload shading and solar array efficiency. This scan axis further describes a slow precession motion around the Sun-to-Earth direction, with an average period of 63 days. Line of sight 1 and 2 represent the position of two telescopes, with basic angle of 106.5° separating them[19].

.

Gaia has four passbands. The G passband from the unfiltered light in the AF, G_{RP} and G_{BP} for red and blue photometers respectively and G_{RVS} in radial velocity spectrometer. The passbands are derived by the convolution of the response curves of the optics and the quantum efficiency curves of the CCDs and are shown in Figure 2.5[16]. The comparison between Gaia, Johnson and SDSS filters can be found in table 2.1.

Due to huge amount of data taken with CCDs, not all is send to the ground. First the Sky Mapper detects the objects, either from telescope one or two. They are distinguished from each other because of a physical mask that is placed in each telescope intermediate image, at beam combiner level. Next, the so called Window (few dozen pixels around the detection, the remaining pixel data is flushed out at high speed) is created and only those are then put through CCDs in the astrometric field. Each object is confirmed by the CCD detectors in the first strip of the AF to eliminate false detections. As the image of the detected object moves across the nine columns, each CCD measures the size, position and brightness. The light then passes through two prisms (RP and BP). For the objects brighter than 17 mag, the light also passes through RVS. It takes about 45 seconds for a source to cross the focal plane. For each object the data collected from all CCDs is compressed into the "data package" and stored in the computer

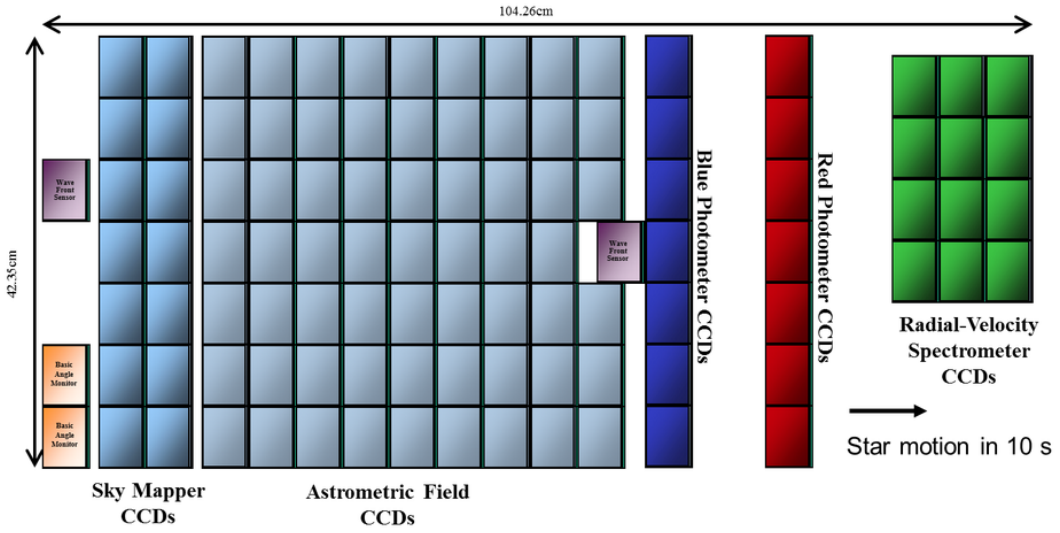

Figure 2.4: Gaia focal-plane assembly, the largest ever developed for space application [16].

	Gaia				Johnson					SDSS				
band	**G**	**G_{BP}**	**G_{RP}**	**G_{RVS}**	**U**	**B**	**V**	**R**	**I**	**u**	**g**	**r**	**i**	**z**
λ_o[nm]	673	532	797	860	361	441	551	647	806	357	475	620	752	899
$\Delta\lambda$[nm]	440	253	296	28	64	95	85	157	154	57	118	113	68	100

Table 2.1: Central wavelength (λ_o) and FWHM ($\Delta\lambda$) for *Gaia*, *Johnson* and *Sloan* passbands [16].

on board Gaia. Since Gaia is visible from the Earth for only 8 hours a day, all data from the last 24 hours is sent to Earth during contact.

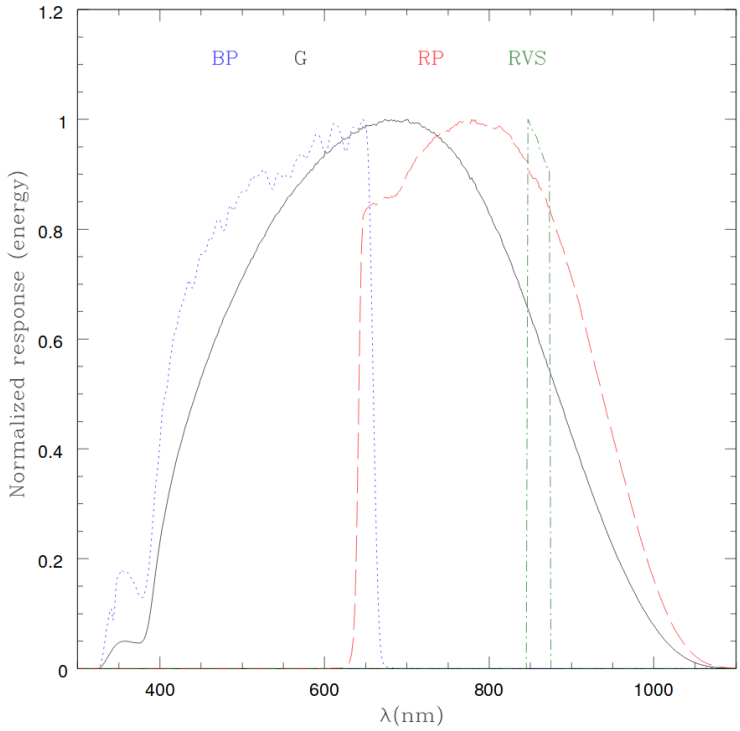

Figure 2.5: Gaia G (solid line), G_{BP} (dotted line), G_{RP} (dashed line) and G_{RVS} (dot-dashed line), normalized [16].

.

2.1.1 Gaia Transient Search

One of many Gaia's science goals is also transient search. The high spatial resolution and precise astrometry and photometry of the Gaia mission makes it a great tool in search for transients. For this the Gaia Science Alerts program was created.

The AlertPipe software is run in the Institute of Astronomy, Cambridge. It operates in two different transient detection algorithms. Transient discovery is based on the detection of:

- *New source*: the event has to have 2 or more observations above flux threshold, G=19, and was not seen by Gaia during previous scans,
- *Old source*: either a source brightened by more than 1 magnitude and this rise is more than 3 sigma above the rms of the historic variations from all data available, or a source brightened by more than 0.15 magnitudes and this rise is more than 6 times the rms of the historic variations from all data available.

After the initial processing, alerts are published from between a couple of hours, and up to 48 hours, after the observation.

Each candidate is analyzed internally, by using available Gaia data. If the object is new, has at least two detections and has no flags for being an artefact, it is labeled as *transient*.

All detected objects are cross-mached with archival databases (OGLE, DSS2, SDSS, Leda, APASS...), to determine if a transient is extragalactic (a galaxy is

present nearby to the position of the alert) or, an orphan transient (if there is no galaxy in the proximity of an alert). In addition to this, spectral pre-classification is done with the Gaia Spectrophotometry Transient Events Classifier (GS-TEC), using data from BP and RP [10]. They are classified into major classes (SNe, CVs, AGNs...). For the magnitudes brighter than 19, around 75% of the transients are robustly classified. For the objects brighter that $G \sim 18.5$ the spectrum can be used for more detail analysis. In case of a SN Ia, providing their estimated redshift with errors $\sigma_z \leq 0.01$ and epoch to peak brightness with error $\sigma_t \simeq 13$. Because classification is not precise enough (due to low resolution of the spectrum) further follow-up observations are crucial.

2.2 OGLE

The Optical Gravitational Lensing Experiment (OGLE) is Polish long-term science project that started in 1992 and has been in operation ever since. At the beginning it's main scientific goal was search for the dark matter with microlensing phenomena (OGLE-I: 1992-1995). Over the years the research got extended to study stellar clusters, AGNs, variable stars, cataclismic variables and transients. OGLE has been among the largest variability surveys providing hundreds thousands variable objects of all types and various transients [26].

Figure 2.6: OGLE survey telescope at Las Campanas Observatory, Chile.

In 1997 the OGLE survey started using 1.3-m Warsaw Telescope, located at the Las Campanas Observatory, Chile, and is operated by the Carnegie Institution for Science. Since then, there were multiple upgrades, the latest one with a 2.5 Megapixel mosaic camera with 32 CCDs (one of the largest CCD cameras worldwide used for astronomy), marking the start of OGLE-IV phase. The mosaic covers the whole 1.4 deg^2 field of view. Each CCD is a 4000×2000 pixel E2V detector, with 15 μm pixels, giving 0.26 arcsec/pixel scale at the focus. The telescope is equipped with Johnson's filters (table 2.1), and OGLE-IV uses only I and V bands, with majority of observations done in I filter. For typical seeing condition of Las Campanas Observatory (about 1.2"), the limiting magnitude is about 20 in I-band. For exceptionally good seeing (less than 0.9") the limiting

magnitude can go down to 21 mag and can reach ≈22 mag in a 150 s exposure [25].

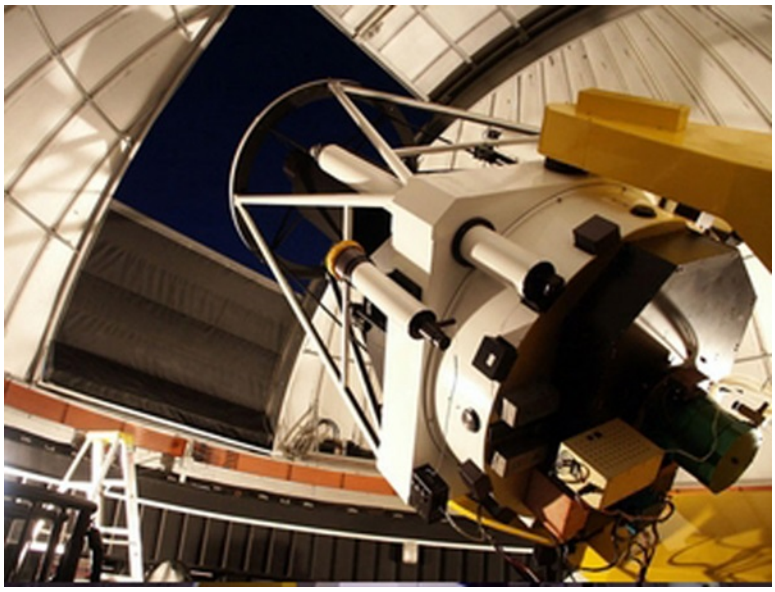

Figure 2.7: OGLE's 1.3-m telescope [27].

OGLE is not an all-sky survey but only monitors the Galactic bulge (BLG), Galactic disc, Large and Small Magellanic Clouds (LMC and SMC respectively) and the Magellanic Bridge (MBR). (Figure 2.10) The regions of the sky are divided into 475 fields and observed with different cadence from 10-30 times per night up to observations every other day or occasional visits. The SMC and LMC sections are typically observed with frequency as high as 4 days. The cadence also varies through the season, depending on the region.

In October 2012 the real-time processing pipeline started to be used regularly, enabling the search for transients in OGLE-IV data. All the data is reduced within 2-16 hour time frame after the end of a night. All data reduction is done at the telescope site in near real-time. Three data pipelines are a real-time software allowing image preprocessing, main photometric reductions of collected images and fast, almost on-the-fly photometry of selected objects [17].

First there is de-biasing and flat-fielding. The data is then processed by OGLE real time photometric pipeline. To make data processing easier, images from each CCD of the mosaic camera are stored as individual FITS files (with the number of CCD in the file name: 01-32) as shown in Figure 2.8. The files are then put in OGLE-IV main photometric data pipeline. It is based on the Difference Image Analysis (DIA) technique with some implementation of Alard and Lupton algorithm. The key element in DIA method is a set of good quality reference images. This is achieved prior to the real-time processing, with combining several images obtained in excellent seeing conditions. The pipeline subtracts each individual FITS file with corresponding reference image. It then selects those subtraction residuals which are of positive sign which means they were caused by brightening. The match to Gaussian profile of PSF profile of brightening must exceed 0.7 (where 1.0 means perfect mach) to classify it as a candidate *new object*. The residuals also have to be present on at least two subsequent frames at the same location. As for the *old sources*, they are classified as objects which were already

visible on previous detections and changed their brightness. The limiting magnitude for the old sources is 18 mag, to eliminate detected variable stars that would be otherwise produced by the pipeline.

All candidates are put through Image Recognition Classifier that reduces the number of candidates by a factor of two, eliminating most obvious and common artifacts, mostly cosmic rays. The final elimination is done by visual inspection of both the images and light curves. The final candidates are published on http://ogle.astrouw.edu.pl/ogle4/transients/.

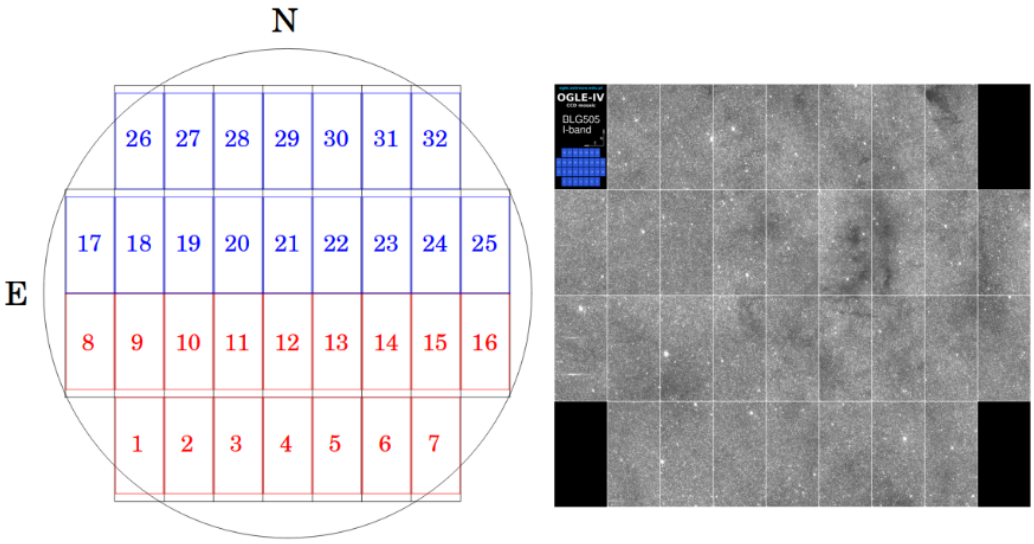

Figure 2.8: Focal plane, filled with E2V 44-82 CCDs (left). Circle represents field of view of the telescope. N and E indicate the directions on sky images. Mosaic camera image of the BLG505 field is shown on the right [25].

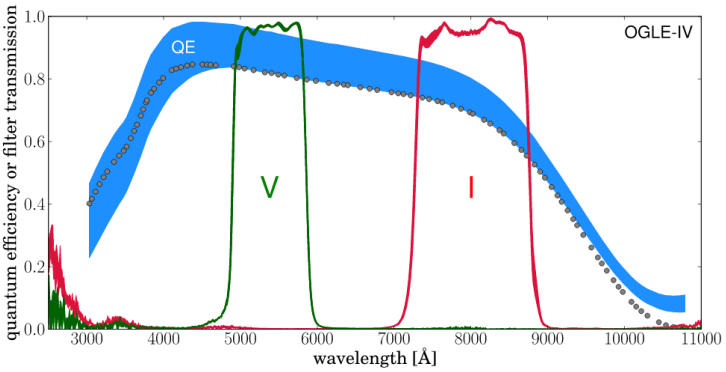

Figure 2.9: Pass-bands of OGLE-IV filters and quantum efficiency (QE)of the CCDs [26].

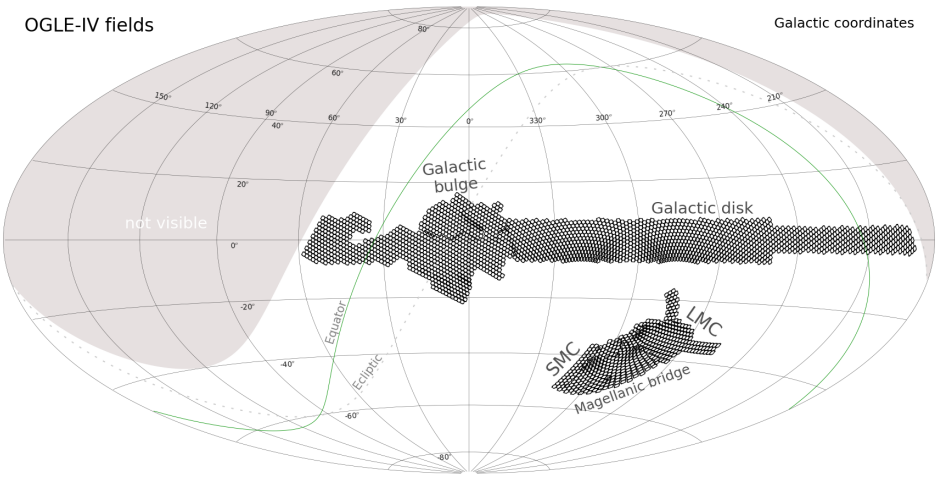

Figure 2.10: Coverage of OGLE-IV sky. Circles represent 475 fields [26].

2.3 Follow-up observations

For the classification of the transients detected with Gaia and OGLE, the follow-up spectroscopic and photometric observations are crucial. Thanks to the OPTICON FP7 EC's grant and HORIZON 22, the long-term multi-band photometric follow-up network has been set up. My work during the preparation of this thesis was carried out as a part of the OPTICON's follow-up network.

Depending on the brightness and the visibility of the discovered transient the follow-up observations were done on two telescopes, Very Large Telescope (VLT) and The Southern African Large Telescope (SALT).

The Very Large Telescope (VLT) (Figure 2.12) is the most advanced visible-light astronomical observatory, consisting of four Unit Telescopes operated by European Southern Observatory (ESO) and stationed in Paranal, Chile [14]. Each of the telescopes has a 8.2-m diameter primary mirrors and can obtain images of the objects as faint as magnitude 30 in one-hour exposure. The instrument used for the spectroscopy is FORS2 (FOcal Reducer/low dispersion Spectrograph), covering the wavelength range of 330-1100 nm. For the classification spectrum Longslit Spectroscopy mode is used which can reach magnitudes of 24.2-23.3 in R filter with the resolution of R: 260-2600.

The Southern African Large Telescope (SALT) (Figure 2.12) is the largest single optical telescope in the southern hemisphere, located at the South African Astronomical Observatory (SAAO) in the Northern Cape province.[18] The telescope has a hexagonal primary mirror array 11 meters across, comprising 91 individual 1 m hexagonal mirrors. It is equipped with multiple instruments. The spectroscopy is done with long slit Robert Stobie Spectrograph (RSS), with the wavelength range of 320-900 nm, with low to medium resolution spectroscopy (up to $R \sim 5000$ with 1 arcsec slits; $R \sim 9000$ with 0.6 arcsec slits).

Figure 2.11: Telescopes used for classification of transients. Left VLT, right SALT [14][18].

For the most promising candidates, observations with Swift satellite were also made. The Neil Gehrels Swift Observatory, is the NASA space telescope designed to detect Gamma-Ray Bursts (GRBs). It is a multi-wavelength space observatory with three instruments: Burst Alert Telescope (BAT), X-ray Telescope (XRT) and Ultraviolet/Optical Telescope (UVOT), working together to observe GRBs and their afterglows. As part of Penn State University's Mission Operations Center (PSU MOC) Target of Opportunity (ToO) observations can be done with XRT and UVOT. The XRT is a focusing X-ray telescope with a 110 cm^2 effective area, 23.6 x 23.6 arcmin field of view, 18 arcsec resolution, and 0.2-10 keV energy range. The UVOT is a diffraction-limited 30 cm (12" aperture) Ritchey-Chrétien reflector, sensitive to magnitude 22.3 in a 17-minute exposure with a field of view of 17 x 17 arcmin and a wavelength range 170-650 nm.

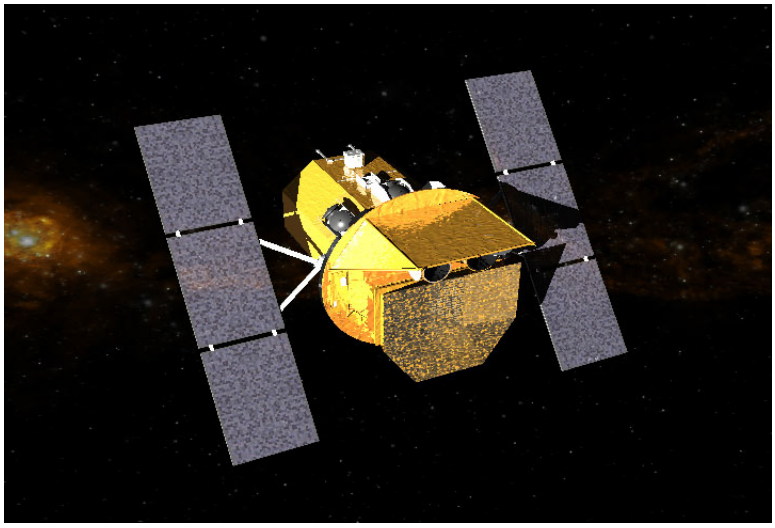

Figure 2.12: Swift spacecraft [20].

Figure 2.13: Locations of VLT and SALT.

3 Visual inspection and automatic analysis

The goal of my research was to detect and study as many nuclear transients as possible in the search for potential TDEs. Because they occur in other galaxies I had to look for them in all parts of the sky. For this, Gaia was a great solution, since it is an all-sky survey. Nevertheless, OGLE survey has its advantages, because the cadence for the visits is higher than for Gaia and has quicker response time from the detection of the transient to its publication.

As mentioned before, I was using Gaia Photometric Science Alerts and OGLE-IV Rapid Transient Detection System. In the next chapters I will sometimes use abbreviations Gaia and OGLE when writing about these systems and not their full names.

This chapter presents the steps taken to identify candidates for further observations.

3.1 Visual inspection

In the beginning of my observational work, I was going through all the targets (all the data) provided by both surveys and eliminating step by step the ones that I was not interested in, the so-called "eye-balling technique". There are of course differences in the way that Gaia and OGLE present their findings, but the basic principles behind my elimination process was practically the same.

At first I had to check the position of the targets. Since I was interested in nuclear transients, I automatically discarded those that didn't occur in a galaxy. For OGLE data, this part was fairly easy due to the fact that OGLE pipeline finds the closest galaxy to the target and provides you with the distance (in unit of arcsec) from the centre of the same line of sight as lies a galaxy to the position of the target. As for Gaia targets, I checked the comment section for each alert and further examined the ones that mentioned that the transient occurred in the same line of sight as lies a galaxy.

The next steps were different for each survey, so I will describe them separately.

3.1.1 Gaia

Upon finding alerts fitting the upper description, I had to check them each individually. Gaia Photometric Science Alerts pipeline produces detailed webpage for each alert as seen in Figure 3.1.

First I checked the location of the alert in the area marked in the Figure 3.1 as *a)*. Image of the galaxy (the base image) is from DSS catalog[1], though one can choose base image layer from multiple catalogs. Based on the size of the galaxy (the size of the square corresponds to FoV=21.89" in the case of Figure 3.1 and is

[1] http://archive.eso.org/dss/dss

changeable, the blob in the middle represents galaxy) and the position of transient (pink + in the centre), I evaluated whether or not it occurred in the nucleus of the galaxy. Because galaxies lie far away it is difficult to determine their centre, so this part was not really precise, but if locations fairly matched, I assumed it was nuclear transient. I usually used the ones, that were approximately $\frac{1}{4}$ of the size of the galaxy away from the supposed centre.

On the right side of the image there is more information about each target; identification name in Transient Name Server (TNS)[2], RA, dec and galactic coordinates, alerting date and time (also in Julian form), alerting magnitude (magnitude that alerted the pipeline), historic magnitude (magnitude of previous detections before the alert if any), classification of the alert if previously known, publication date, information on other surveys detections, comments (about the alert, based on which I initially choose the target) and if previously observed and published the ATels (The Astronomer's Telegram, an internet based short notice publication service for quickly disseminating information on new astronomical observations).

The section marked with *b)* shows the lightcurve of the event. The black circle represents alerting magnitude and the blue ones magnitudes of other detections.

The section *c)* shows the low resolution spectra (BP, RP) taken at the time of the alert and next detections. Based on this I determined if the transient is a potential candidate for TDE and therefore interesting for follow-up observations. I was looking for blue continuum spectra which indicates high temperatures with the shape similar to the one in Figure 3.1.

Lastly I checked in NASA/IPAC Extragalactic Database (NED)[3] to see if there is a known redshift to the host galaxy. With this, I could calculate the absolute magnitude of the target and from that distinguish TDE candidates from all others (since they are the most luminous of all visible light transients with absolute magnitude of -20 up to -23 mag).

For the transients that successfully passed these steps I checked for the visibility and based on this decided which telescope to use for follow-up observations.

[2] https://wis-tns.weizmann.ac.il/
[3] http://ned.ipac.caltech.edu/

Figure 3.1: Example of page produced by Gaia Photometric Science Alerts for a TDE candidate.

3.1.2 OGLE

As mentioned before, OGLE pipeline produces page with list of observed targets. An example of a target is shown in Figure 3.2 which shows orphaned SN.

Under the images there is a description with all the information regarding the target. The name of the target, position (RA, dec), HOST (name of the host galaxy or the closest galaxy to the target with the distance from the centre of the host galaxy in the brackets in arcsec), the name and the number of the field with the number of CCD which detected it, date (HJD[4]) of observation, magnitude of the target and the time of the discovery.

The graphs marked with *a)* show the evolution of the target's *I-band magnitude*. The image marked with *b)* shows the reference image, *c)* the image of the detection and *d)* subtracted image. The bottom three images are just zoomed *b), c), d)* images respectively. The images are FITS files, which can be downloaded to check for the Point Spread Function (PSF), to see if it is a real target and not an artifacts (Figure 3.3). Because OGLE is a ground based observatory, there are numerous "fake" transients, from bad subtraction and bad parts of the image (Figure 3.4), cosmic rays (Figure 3.3), satellite tracks and flares from bright stars (Figure 3.5), to fast moving bright stars (Figure 3.6).

For the transients that were left after elimination of fake transients, I checked their visibility and based on this decided which telescope to use for follow-up observations.

[4]Heliocentric Julian Date is the Julian Date corrected for differences in the Earth's position with respect to the Sun

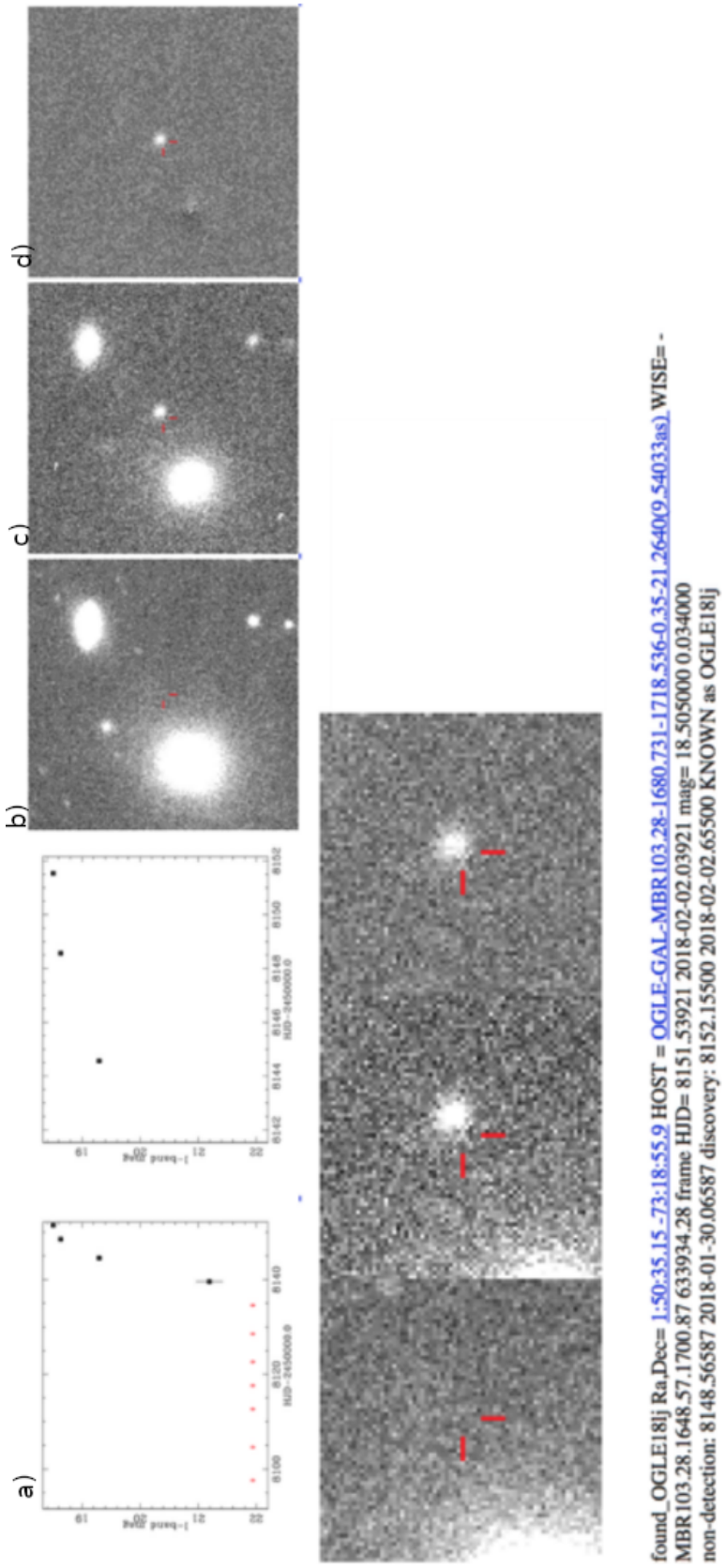

Figure 3.2: Example of all the data shown for a target with OGLE pipeline.

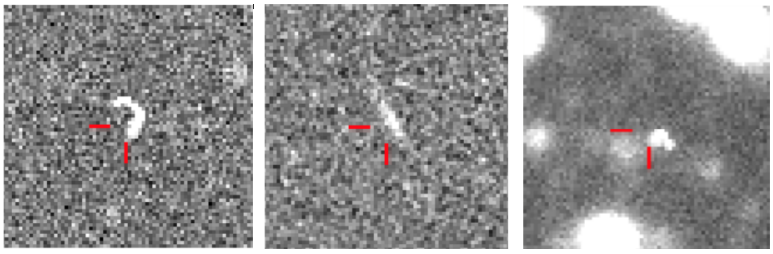

Figure 3.3: Examples of cosmic rays detected with OGLE, which I had to remove from the list of transient candidates. Left and middle one are obvious as they are not spherical. Upon checking for PSF of the one on the right it was obvious from the shape of the curve that it is a cosmic ray.

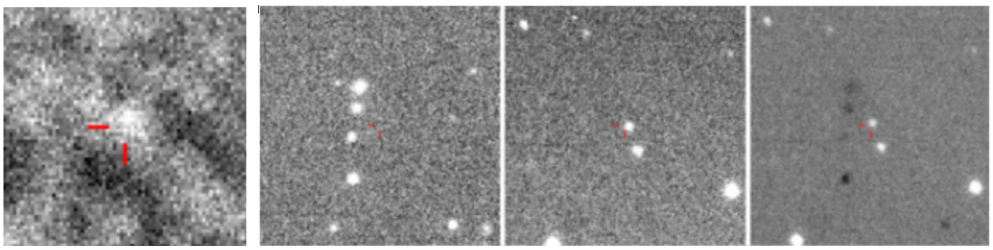

Figure 3.4: Example of bad parts of the image which is seen as not homogeneous background resulting in black and white patches the later detected as a new target (left) and bad subtraction (second image is the reference image, third is observed image and forth subtraction of previous two. Because the reference and the observed images are not at the same position (the frames are shifted), the subtracted image shows a new transient but is in fact not).

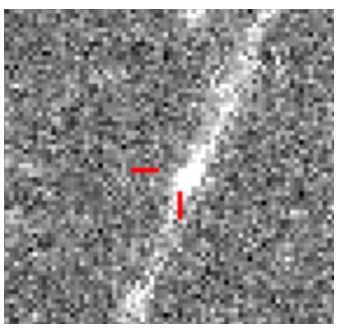

Figure 3.5: Example of subtracted image with satellite track in it.

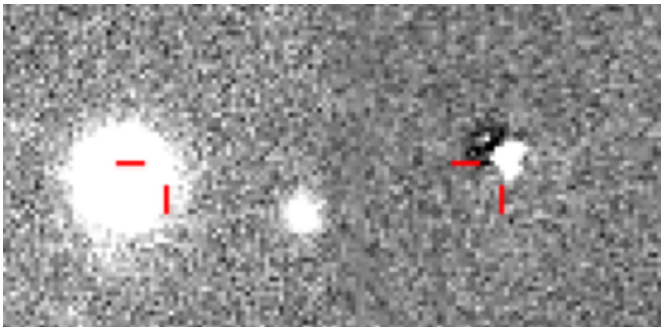

Figure 3.6: Example of a bright star detected as transient. Left image represents the observed image and the right one subtracted image. The black area means that that part is darker than it was in reference image, which is not possible since some part is brighter than before. Also the current image was shifted which produced black and white areas.

3.2 Automated selection in Gaia

I decided to ease my work and tried to automatize the search for nuclear transients detected with Gaia. I wrote a code using Python 2.7. which is run on thousands of alert candidates from Gaia and filters them for nuclear candidates.

The code basically follows the steps that I did manually with some exceptions. I put the limit on galactic latitude, meaning I excluded the region between -15 deg and + 15 deg because I am interested in extragalactic targets and same on ecliptic plane (±15 deg) so that the Sun could not affect possible follow-up observations. And in those parts of the sky the field is crowded with stars and objects from our Galaxy, so the probability to detect transient from other galaxies is small. I fixed the search radius of 1.05 arcsec from the centre of the presumed host galaxy meaning that if the transient lies outside this radius it gets discarded. So, first the code reads the coordinates of the target. Then it compares them with the data from several catalogs from different surveys:

- The Lyon-Meudon Extragalactic Database (**LEDA**[5]): It is a database of galaxies that provides homogenized description of observable and physical properties of galaxies.
- The Sloan Digital Sky Survey (**SDSS**[6]): It is detailed three-dimensional map of the Universe with deep multi-colour images of one third of the sky.
- The Panoramic Survey Telescope And Rapid Response System (**Pan-STARRS**[7]): A system for wide-field astronomical imaging with first data release as PS1.
- The Dark Energy Survey (**DES**[8]): It is a growing catalog of a hundreds of millions of galaxies with the aim to find patterns of cosmic structure that will reveal the nature of the dark energy.

In all catalogs the parameters that I was interested in were coordinates of galaxies and their size.

The next step is based on the magnitude of the object. To eliminate all the variable stars I put the upper limit magnitude of 16.6 mag and to dispense with all the potential supernovae the lower limit of about 19.2 mag. Both limits were necessary because, based on the criteria that I used in catalogs to determine if transient occurred in the nucleus of a galaxy, it was not possible to distinguish galaxies from stars and since star varies in the centre the code marked them as nuclear transients. As for the lower limit, TDEs are bright objects and also the telescopes for the follow-up observations have a limit which they can observe.

The final step is the creation of the web page with all the data.

The final product of the code is a web page (shown in Figure 3.7 and 3.8), with all the essential data: the map with the position of all detected transients (before they are put through the code), the number of targets, following the

[5] http://leda.univ-lyon1.fr/
[6] http://skyserver.sdss.org/dr14/en/home.aspx
[7] http://archive.stsci.edu/panstarrs/search.php
[8] https://www.sdss.org/dr12/data_access/

number of targets that remain after every cut. And lastly the table with the nuclear targets and all crucial data: light curve, image of host galaxy taken from reference catalogs with the position of occurred transient, blue and red low resolution spectra, coordinates and links to more extended information received from Gaia for the particular transient.

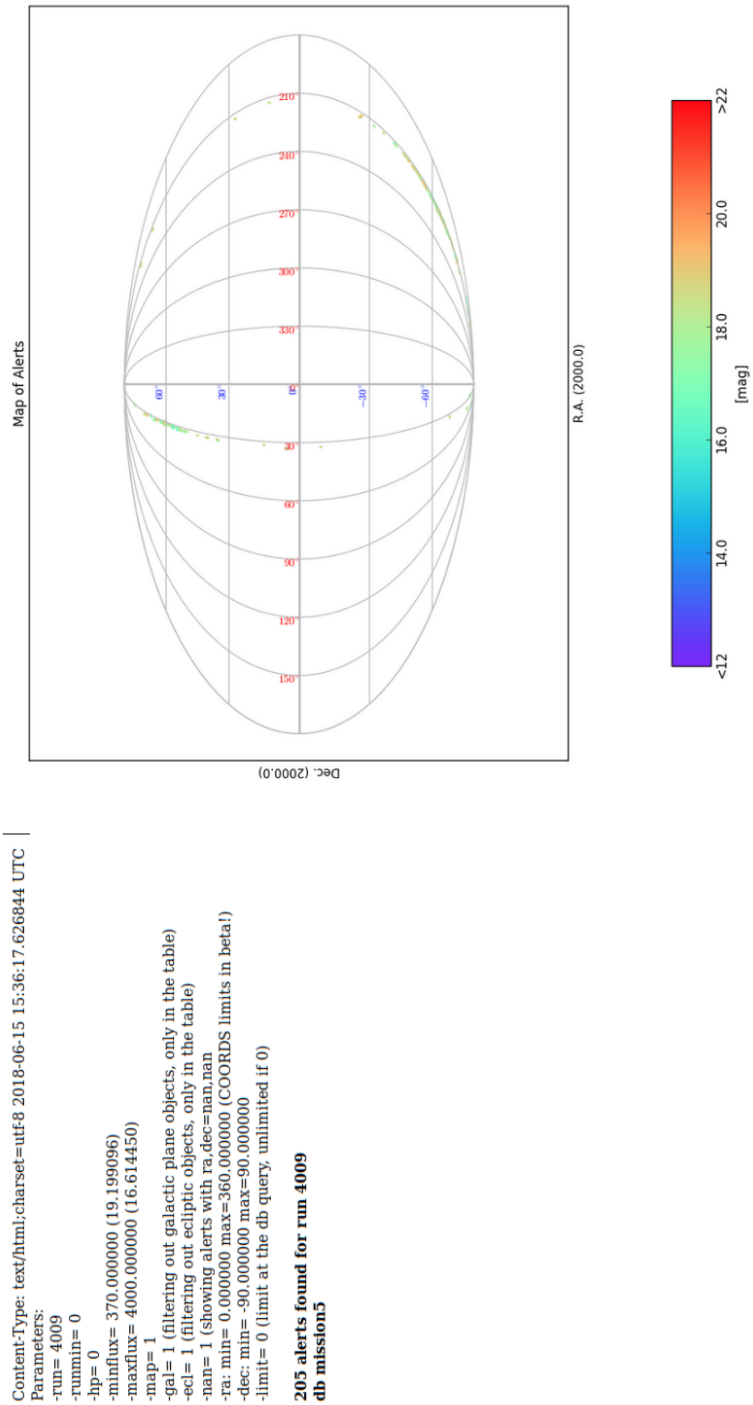

Figure 3.7: Example of the final product of my code with one detected nuclear transient. Because of the size of the web page, it is shown in two separate figures.

Figure 3.8: Second part of the produced page.

4 Results

This chapter represents the results of the work done in six months observation period, from September 2017 to March 2018. In this time there were around 40 nuclear transients detected with both surveys. However, ten of them were either already detected with previous surveys and classified or their host galaxy had a known redshift, from which I could calculate the absolute magnitude that turned out to be too small for a TDE. Around five of them were pre-classified as SNIa with GS-TEC [10] and 16 were not visible from any telescopes that were available for our follow-up observations. For the remaining nine nuclear transients, we got further photometric and spectrometric follow-up observations from VLT, SALT and Swift (for some cases) and are presented in the following sections.

The data processing was done with multiple pipelines and programs. The selection of potential TDE candidates and use of different techniques is described in previous chapter. For the visibility check, I used ESO's pipeline for VLT and SALT target visibility. All data analysis was made with Image Reduction and Analysis Facility (IRAF), a general purpose software system for the reduction and analysis of astronomical data.

Classification of transients was done with two different softwares; *Supernova Identification (SNID)[22]* and *DASH[23]*. They both fit the given spectrum to all known types of SNe based on the shape of spectrum and spectral lines and give the best fit. First, the classification was done using these softwares. For six of them, SNID identify them as SNe, for the rest of them, the classification was inconclusive. Therefore further observations were necessary with Swift. DASH classification produced the same results with one exception. One of the SN was classified with SNID as Ia and as IIb with DASH.

Figure 4.1: Diagram shows number of classified nuclear transients in this work with SNID code.

The Table 4.1 lists all nine nuclear transients which were found and further studied during this work, from both Gaia and OGLE surveys, along with their

properties. *Al. mag* means alerting magnitude of transient, where Gaia's magnitudes are in Gaia's *G-band* and OGLE's is in Johnson's *I-band*. As for *abs mag*, this value for OGLE transients means peak absolute magnitude of the transient, where for Gaia's transients it is the upper limit for absolute magnitude of the transient (it is a magnitude of a transient in a galaxy). For calculating absolute magnitude I used cosmological model with Hubble constant $H_o = 72\frac{\mathrm{km/s}}{\mathrm{pc}}$ and density parameter $\omega = 0.3036$[21]. It has to be also taken into an account that OGLE's alerting magnitude is the actual magnitude of the object because the measurements are only from the flare due to the possibility of automatic image subtraction, so the absolute magnitude in the table is the peak magnitude of the transient. On the other hand, this can not be said for Gaia data. Gaia's magnitudes are not host galaxy subtracted, therefore the absolute magnitude in the table is actually upper limit for the transient. In addition, magnitudes are not corrected for galactic and host galactic extinction.

								classification	
Name	**RA, dec**	**TNS name**	**survey**	**al. mag**	**abs mag**	**follow-up**	**redshift**	**SNID**	**DASH**
Gaia17cen	05:05:44.39 -23:23:50.93	AT2017gld	Gaia	20.56	-19.09	SALT	0.077	SN Ia	SN Ia
Gaia17cmd	07:41:45.5 +16:13:06.10	AT2017har	Gaia	18.38	-20.11	VLT, Swif	0.110	AGN flare	
OGLE17hil	05:57:30.04 -62:28:44.60	AT2017hil	OGLE	18.56	-18.59	VLT	0.061	SN Ia	SN Ia
Gaia17dbg	22:54:13.35 -21:41:00.08	AT2017gul	Gaia	18.35	-21.45	SALT, VLT, Swift	0.192	TDE ?	
Gaia17cqz	21:47:57.52 -58:10:58.12	AT2017hrw	Gaia	18.85	-16.39	SALT	0.026	SN IIp	SN IIp
Gaia18aql	16:07:15.74 +26:11:48.05	AT2018zo	Gaia	18.49	-18.37	VLT	0.054	SN Ia	SN Ia
Gaia18aoq	13:55:07.91 -38:23:22.74	AT2018aev	Gaia	18.61	-16.63	VLT	0.026	SN IIp	SN IIp
Gaia18aeo	03:06:37.26 -36:37:05.92	AT2018ig	Gaia	18.25	-19.61	SALT	0.086	SN Ia	SN IIb
OGLE18wc	05:18:11.72 -51:44:03.97	AT2018wc	OGLE	19.915	-20.22	VLT, SALT, Swift	0.220	blazar	

Table 4.1

4.1 Gaia17cen

Gaia17cen also known as AT2017gld was discovered by Gaia Science Alerts pipeline on 2017-09-02, at coordinates RA= 05:05:44.39 and dec=-23:23:50.93, with the alerting magnitude of 18.46 mag in what looked like in the nucleus of the host galaxy GALEXASC J050544.48-232351.7. At the time it was visible with SALT, so we requested a spectrum.

A low resolution (R = 350) SALT/RSS spectrum was taken on 2017-09-10, under the SALT Large Programme on transients (2016-2-LSP-001).

The spectroscopic classification was initially done using SNID code and it was matched to SN Type Ia-91T at about 15 days past maximum as shown in Figure 4.2. For re-checking I also did classification with DASH which also matched to SN Ia-91T.

Spectrum on Figure 4.4 shows narrow emission Hα line which is present due to the nucleus of the host galaxy. Based on this, I calculated the redshift 0.0768±0.0002. Gaia photometric measurement near the maximum brightness at this redshift corresponds to absolute magnitude of about -19.1 mag, also consistent with SN Type Ia. The absolute magnitude is the upper limit for SN, because it was not possible to subtract the host galaxy because there was no prior detection of this galaxy.

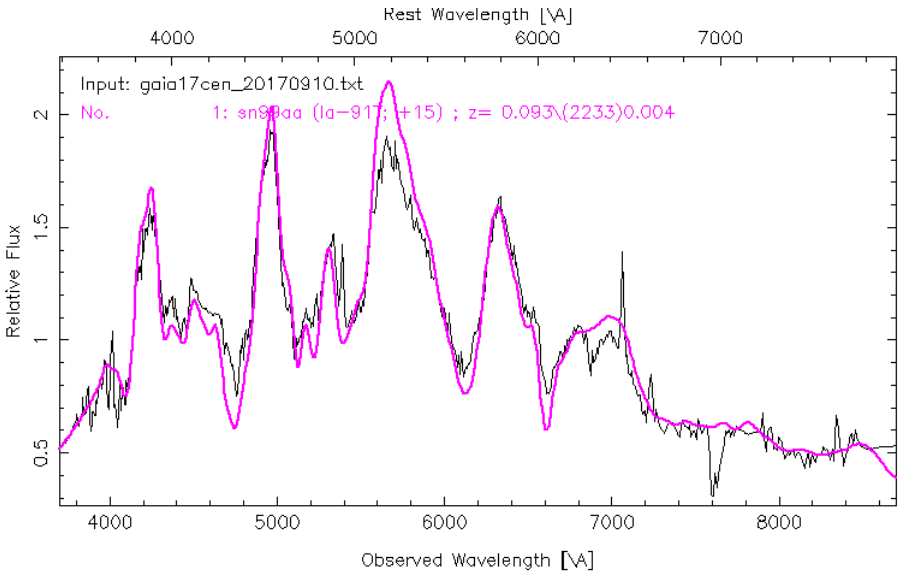

Figure 4.2: Spectroscopic classification of Gaia17cen using SNID code. It is mached to SN Ia-91T, 15 days past maximum. The black line presents spectrum of Gaia17cen and the pink one is the matched spectra.

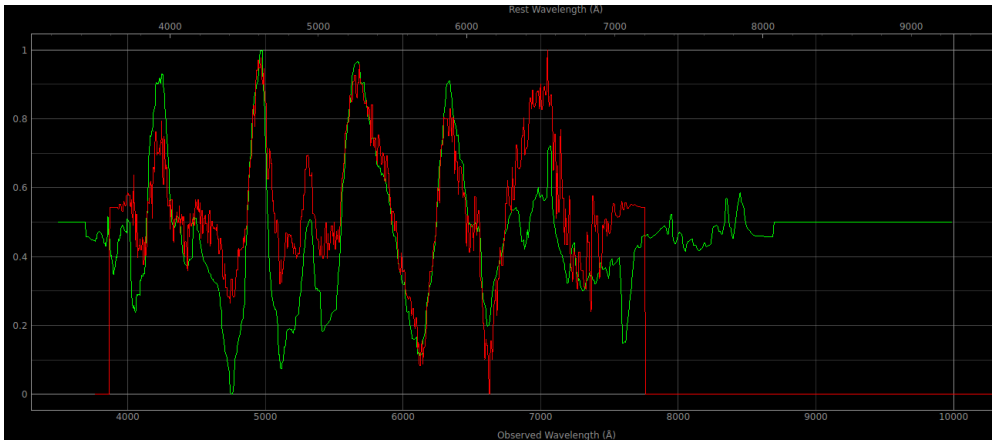

Figure 4.3: Spectroscopic classification of Gaia17cen using DASH code. The green spectrum is SALT sprectra of Gaia17cen and the red one is the match, SN Ia-91T.

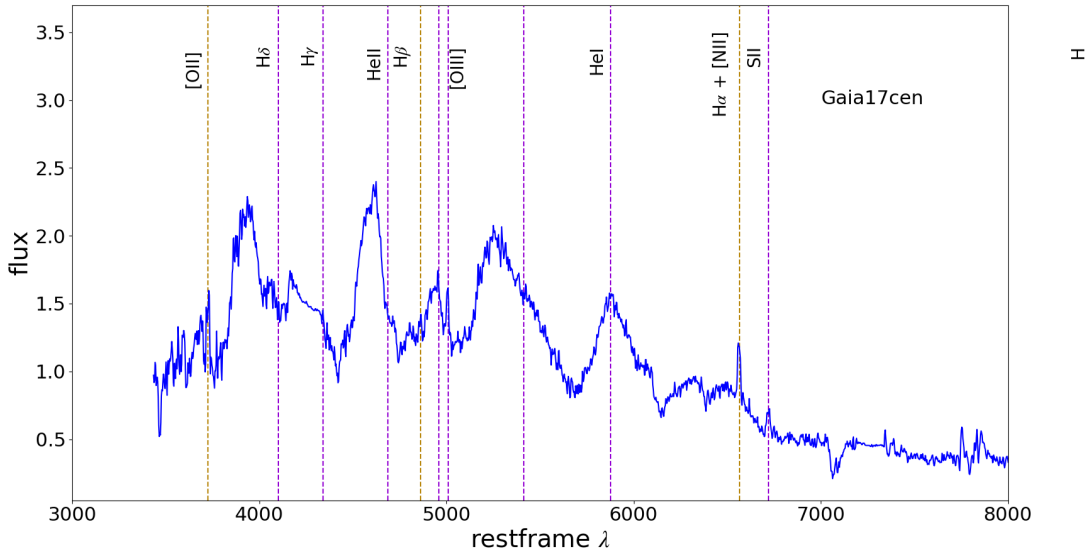

Figure 4.4: Spectrum of Gaia17cen taken by SALT on 2017-09-10.

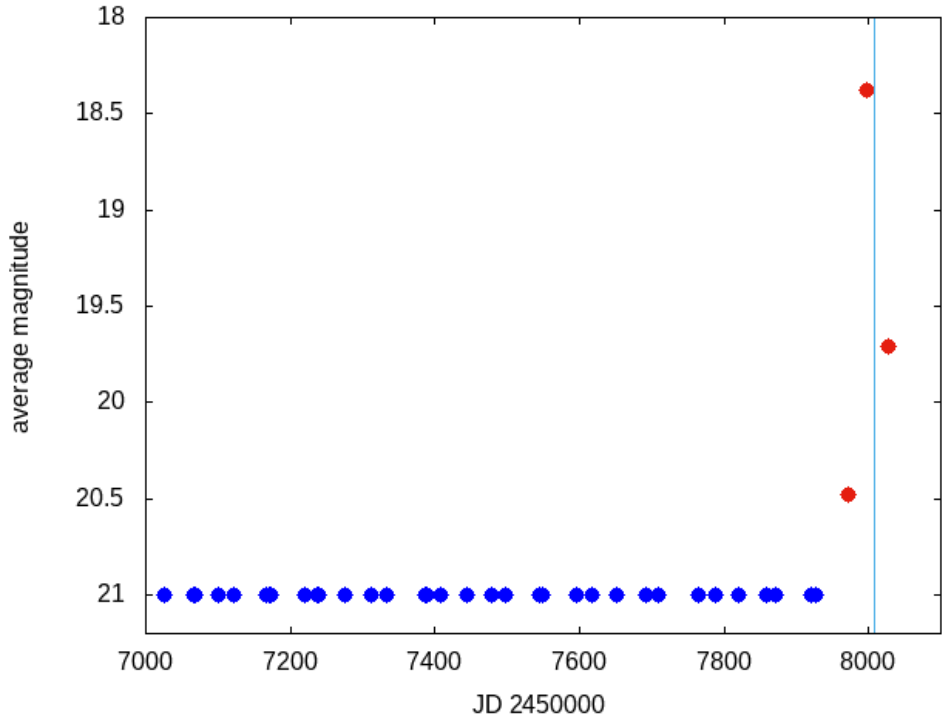

Figure 4.5: Lightcurve for Gaia17cen, with the average magnitude in Gaia's G-band. Red points represent detections and blue ones non-detections. The maximum magnitude is actually double point. The vertical line represents time when the spectrum in Figure 4.4 was taken.

4.2 Gaia17cmd

The optical transient Gaia17cmd was discovered by Gaia Science Alerts program on 2017-09-30 coinciding with the very nucleus of a barred spiral galaxy 2MASX J07414558+1613063 at coordinates RA=07:41:45.5 and dec=+16:13:06.10. Galaxy had almost no change in magnitude before the spike of 0.6 mag rise in the centre of a galaxy (Figure 4.7). The galaxy is suggested to be an AGN based on WISE colours[31], however no X-ray or radio detection has been published. Based on the position, magnitude and visibility we decide for a follow-up observations with VLT.

The spectrum of Gaia17cmd was obtained on 2017-10-05 using FORS2 on VLT because it was not visible with SALT. The spectrum (Figure 4.6) reveals blue continuum with superimposed emission lines of the Balmer series, [N II], SII, [O II] and [O III] at redshift z=0.099±0.0005. I determined redshift based on Hα. Gaia17cmd is very similar to a composite of broad-line AGN (quasars) taken from the Sloan Digital Sky Survey[32], but the iron complex seems to be slightly stronger.

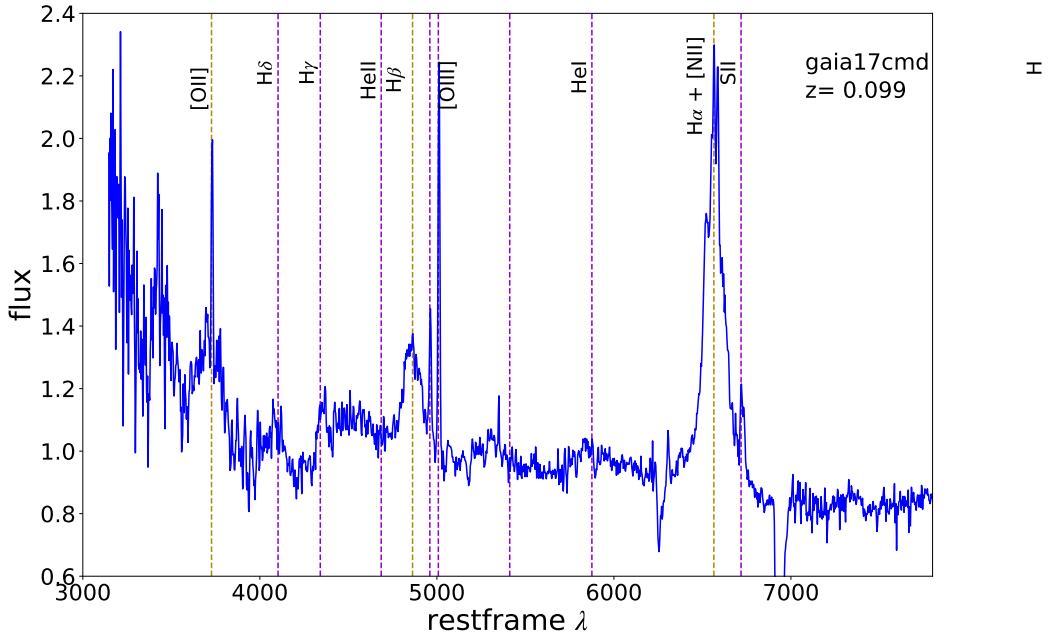

Figure 4.6: Spectrum of Gaia17cmd with spectral lines. At 4500Å lies iron complex. Broadened Hα line indicates high temperatures, typical for most AGNs. Spectrum was obtained with VLT on 2017-10-05.

Gaia17cmd was observed with Swift for 2.1ks on 2017-10-18.

An ultraviolet source was detected at the position of the transient with the following UVOT magnitudes (no host light subtracted):

JD	Band	Mag.	Err.
2458045.29	UVW2	17.39	0.06
2458045.30	UVM2	17.47	0.07
2458045.30	UVW1	17.51	0.07

Taking into account the Galactic reddening of E(B-V)=0.029, these magnitudes suggest a black-body emission with the temperature 20000 K. The high colour temperature together with the X-ray detection, optical spectrum properties and archival WISE colours are consistent with this event being an AGN flare.

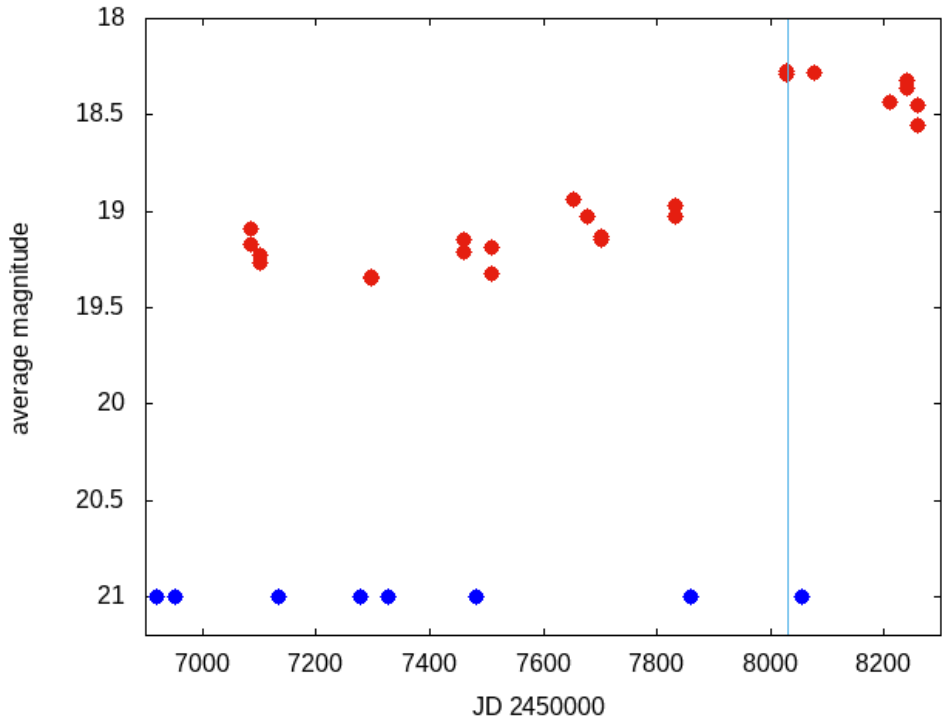

Figure 4.7: Lightcurve for Gaia17cmd. Before the re-brightening , there is slight variability (order of 0.3 mag in 3 years). Red dots represent detections and blue one non-detections, all taken with Gaia's *G*-band. Vertical line represents time when the spectrum with VLT was taken.

4.3 OGLE17hil

The nuclear transient OGLE17hil also known as AT2017hil was discovered by the OGLE-IV Transient Search System on 2017-10-13 at coordinates RA=05:57:30.04 and dec=-62:28:44.60. The host galaxy is a spiral galaxy, OGLE-GAL-LMC605.05-897.374-1129.222, and transient is located very close to the nucleus with only 0.4 arcsec separation.

OGLE17hil was visible with VLT with which we obtained spectrum the next day, on 2017-10-14, using FORS2.

The spectroscopic classification done using SNID code matches to SN Type Ia-norm at about 7 days past maximum. Figure 4.8 displays fitted spectrum. I did another classification with DASH (Figure 4.9) which also matched spectrum to SN Ia. I estimated redshift z=0.0612±0.0002 based on host lines: Hα, [N II] SII, [O II] and [O III] in emission and Hδ, Na and CaII, H and K in absorption. OGLE photometric measurements did not recorded the date of the maximum as it was discovered after the peak magnitude, however at the moment of detection the observed magnitude (18.56) at this redshift corresponds to the absolute magnitude of approximately -18.7 mag which is consistent with SN Type Ia.

The lightcurve in Figure 4.11 shows secondary bump around JD 2458060 which is typical for SN Ia.

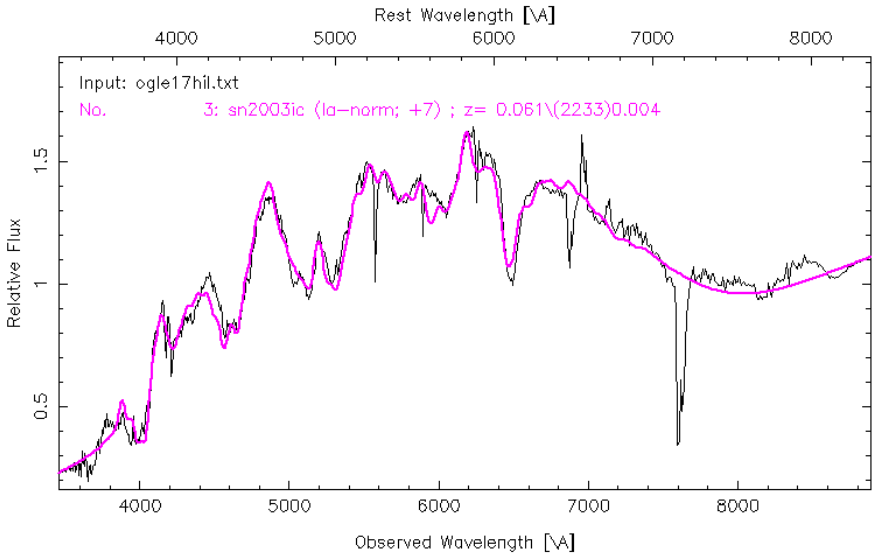

Figure 4.8: Spectroscopic classification of OGLE17hil, using SNID code. Spectrum is shown in black and the fitted one in pink.

The archival OGLE-IV photometry (Figure 4.12) of this host galaxy revealed that there was another (previously undetected) transient near its nucleus in October 2011. Its light curve (shown in Figure 4.13) resembles that of SN Ia, with the secondary bump visible in the I-band.

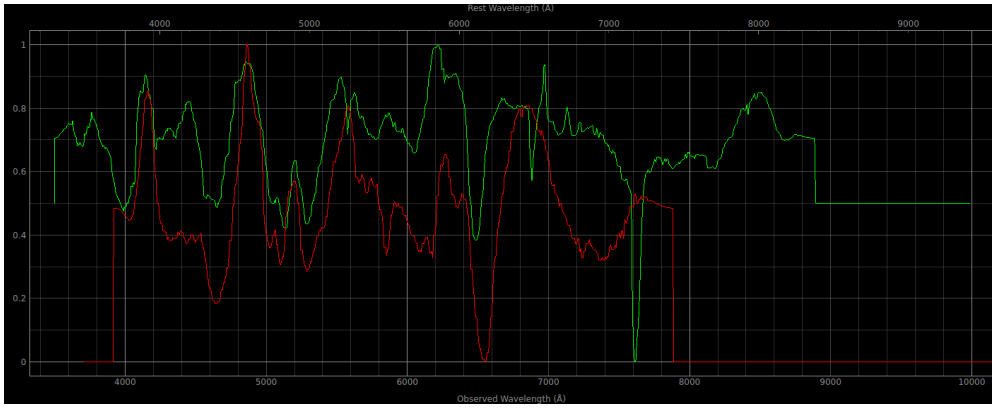

Figure 4.9: Spectroscopic classification of OGLE17hil, using DASH code. Fitted spectrum of SN Ia is in red, green spectrum represents OGLE17hil.

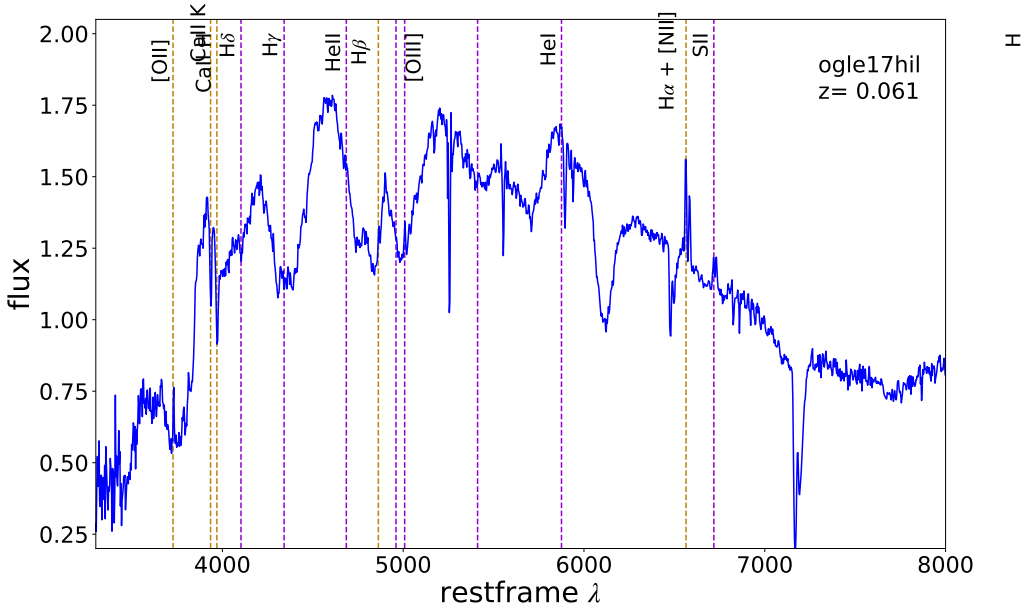

Figure 4.10: Spectrum of OGLE17hil with spectral lines. Spectrum was taken with VLT on 2017-10-14.

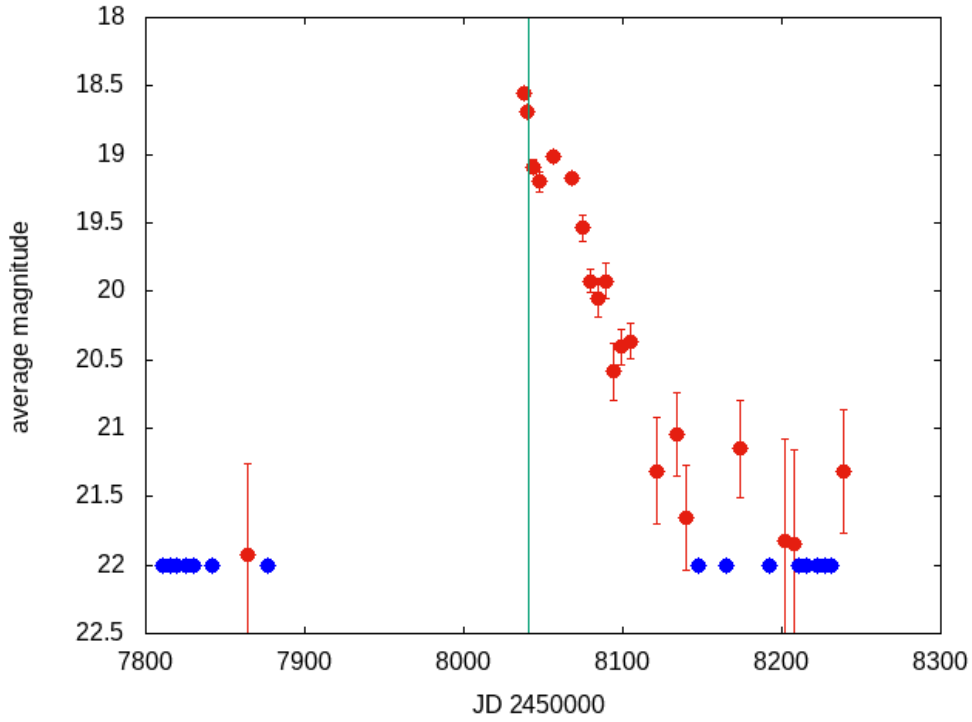

Figure 4.11: Lightcurve for OGLE17hil in I-band. The maximum was not detected, but the secondary bump is nicely visible around time 8060. Blue dots represent non detection and the red ones detection. Vertical line represents time when the spectrum with VLT was taken.

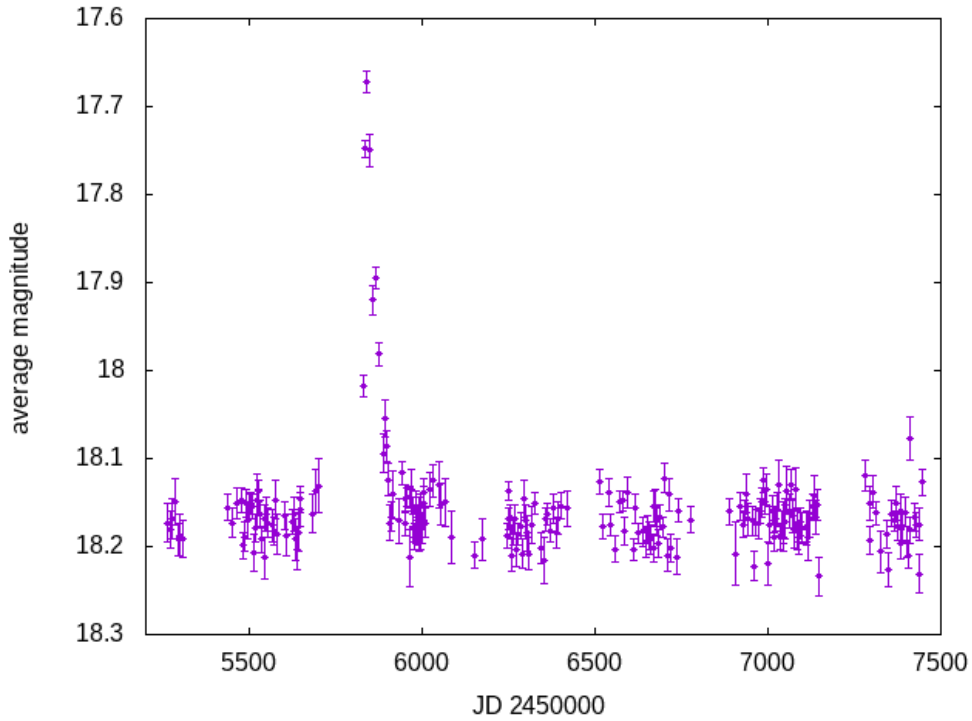

Figure 4.12: Lightcurve of host galaxy of OGLE17hil. It shows unknown transient with its peak on October 4th 2011.

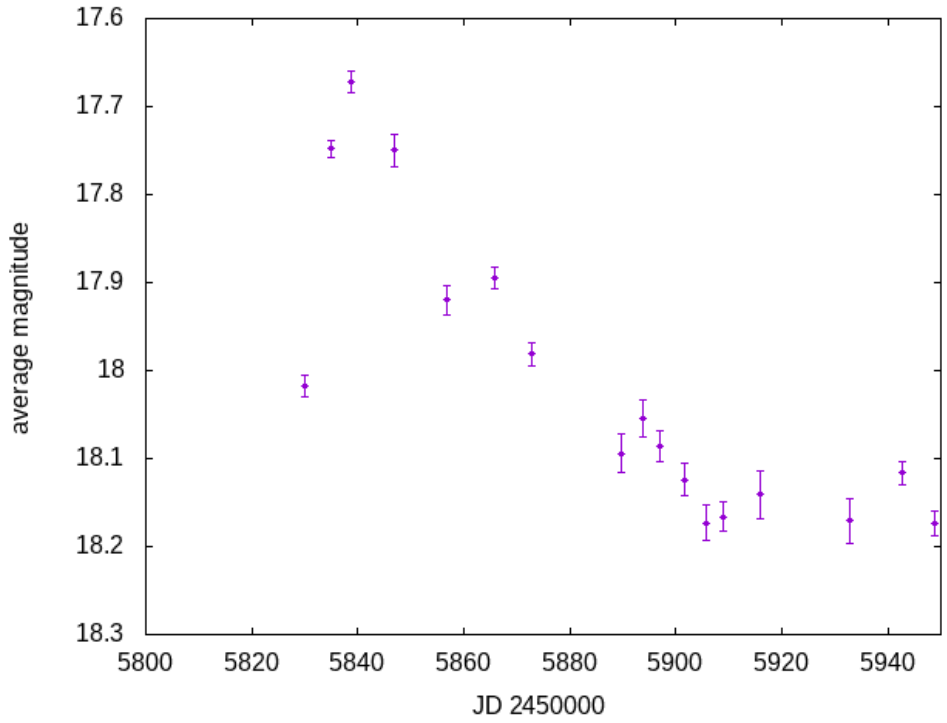

Figure 4.13: Zoomed in lightcurve of the event that occurred in a host galaxy of OGLE17hil in 2011. The secondary bump is clearly visible which indicates that it was possibly a SN Ia.

4.4 Gaia17cqz

Transient Gaia17cqz also known as AT2017hrw was discovered by Gaia Science Alerts program on 2017-10-19 at coordinates RA= 21:47:57.52 and dec=-58:10:58.12. The transient was detected in the nucleus of the host galaxy LEDA 381385 with the alerting magnitude 18.85. Since it was best visible with SALT, low resolution (R = 350) SALT/RSS spectrum was taken on 2017-11-08.

The spectroscopic classification done with SNID code matched transient with SN IIP at about 2 weeks past maximum as can be seen in Figure 4.14. I also did classification with DASH that gave me the same result (Figure 4.15).

The spectrum shows very broad Hα line which is typical for this type of SN. Based on the spectral lines (Figure 4.16) I estimate redshift z=0.026±0.0005. Gaia photometric measurement at the moment of observation and at this redshift corresponds to the absolute magnitude of about -16.51 mag.

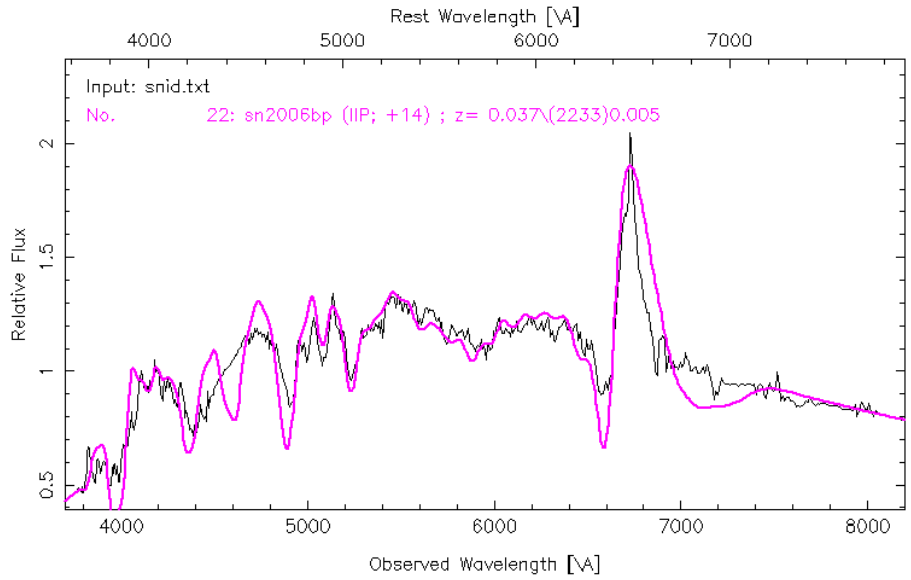

Figure 4.14: Spectroscopic classification of Gaia17cqz (black spectrum), using SNID code. It is matched to SN IIp. The matched spectrum is in pink.

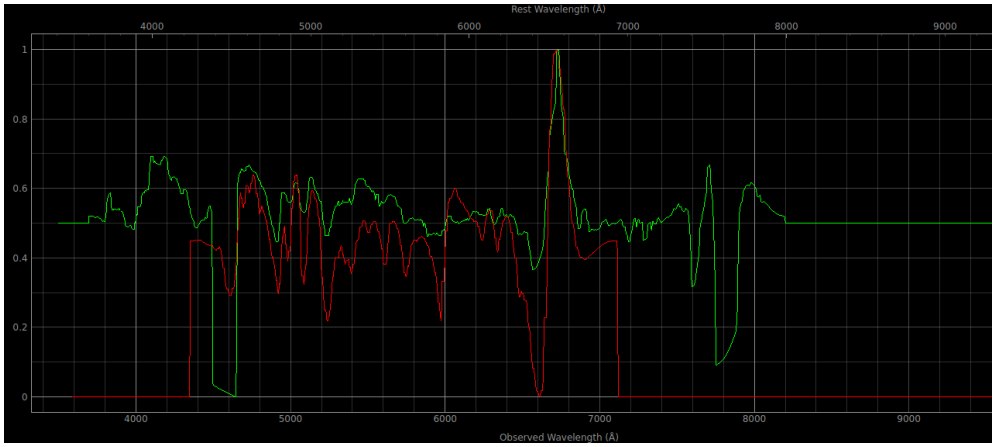

Figure 4.15: Spectroscopic classification of Gaia17cqz, using DASH code.

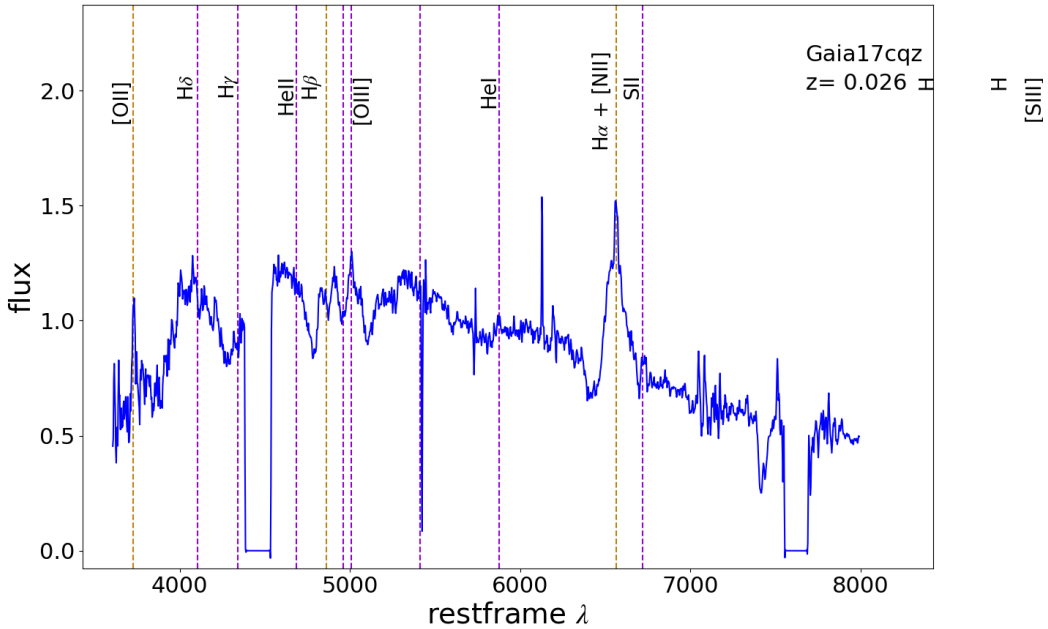

Figure 4.16: Spectrum of Gaia17cqz with marked spectral lines. Spectrum was taken on 2017-11-08 with SALT.

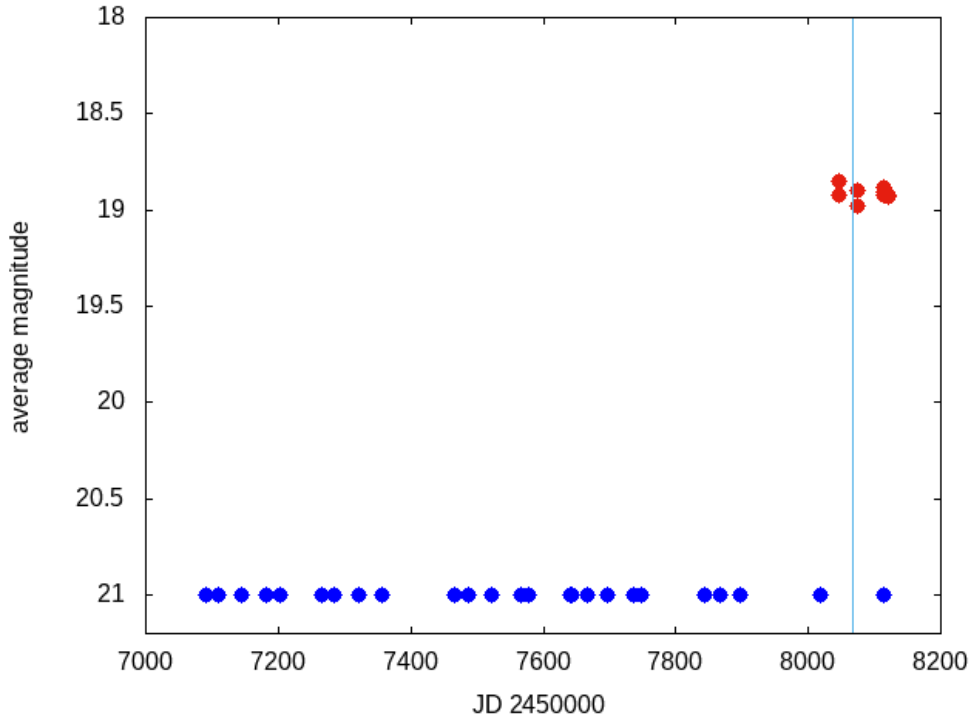

Figure 4.17: Lightcurve for Gaia17cqz with only few points with little variation. Red ones represent detection and blue ones non-detection. Vertical line shows time when spectrum in Figure 4.16 with SALT was taken. Detections were measured with Gaia in *G-band*.

4.5 Gaia17dbg

The optical transient Gaia17dbg also known as AT2017gul was detected by Gaia on 2017-11-25.0, however it was first discovered by ATLAS on 2017-08-01.5 UT as ATLAS17lbg. In Gaia data the latest non-detection was on 2017-07-13. The transient is coinciding with the centre of the galaxy GALEXASC J225413.32-214100.1 at coordinates RA=22:54:13.35, dec=-21:41:00.08.

The first SALT/RSS spectrum of Gaia17dbg was obtained on 2017-11-28.8 (spectral range 370.0-900.0 nm) with an (averaged) spectral resolution of 350 and exposure time of 1200s. The slit of spectrograph cut out Hα line, so additional spectra were needed. The spectrum consists of blue continuum with superposed Balmer, [OII], [OIII], [NIII], [SII], HeII 468.6 nm and HeI 578.6 nm emission lines at z=0.192.

The second spectrum was obtained on 2017-11-29.8 (spectral range 518.7-821.4 nm, R 1100, 1200s exposure). It revealed extremely powerful Hα+[NII] line, H-beta and HeI emission lines composed of unresolved (<350 km/s) and resolved (FWHM 2500 km/s) components (Figure 4.18).

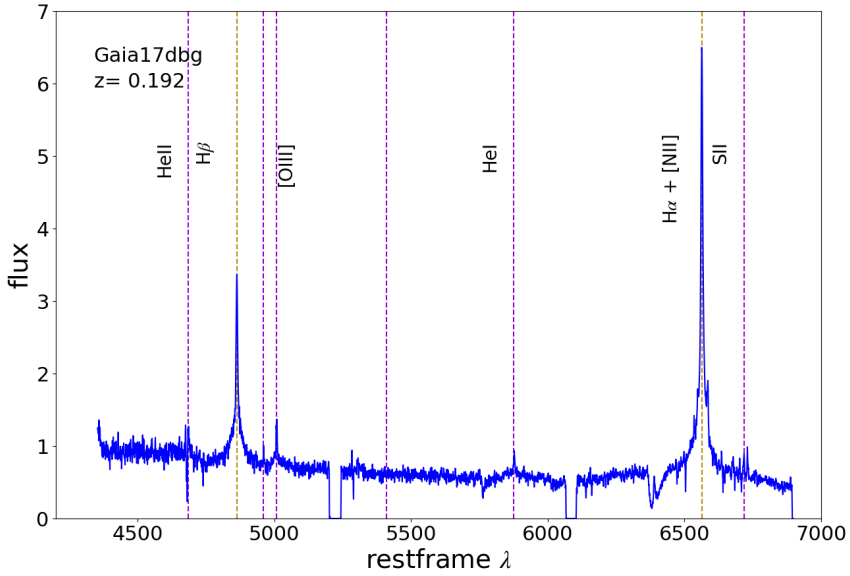

Figure 4.18: Spectrum of Gaia17dbg obtained on 2017-11-29 with SALT, with marked spectral lines.

Additional spectrum was taken wit FORS2 on VLT, 2017-12-22. Spectrum is shown in Figure 4.19.

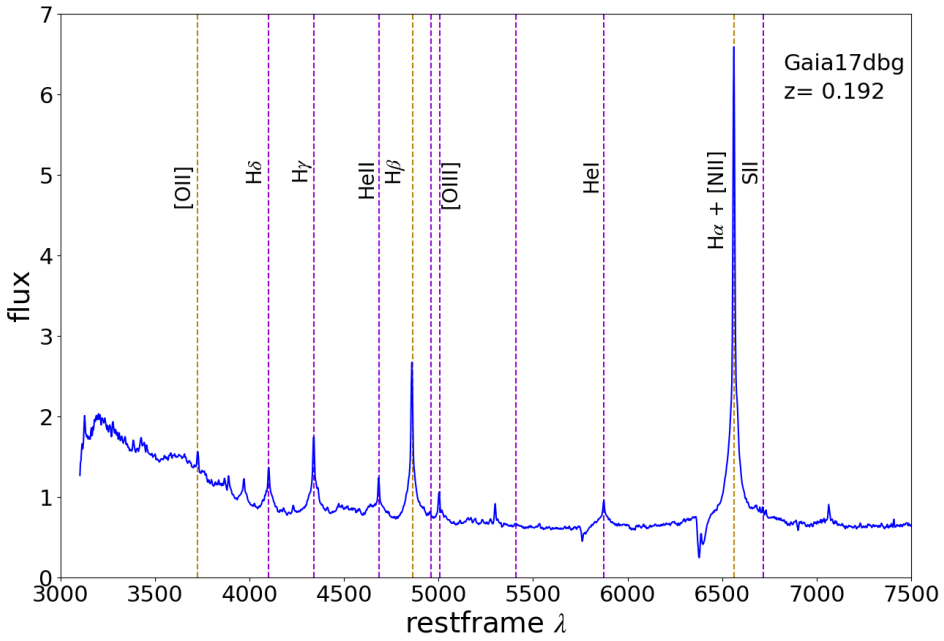

Figure 4.19: Spectrum of Gaia17dbg obtained on 2017-12-21 with VLT, with spectral lines.

Swift observed Gaia17dbg for 1.8ks on 2017-12-05.6. Swift/XRT detected no X-ray source at the position of the transient with an upper limit of 0.004 +/-0.002 cts/s.

An ultraviolet source was detected at the position of the transient with the following Swift/UVOT magnitudes (AB system), suggesting a brightening with respect to the archival GALEX detection at NUV=21.1 +/-0.2. Taking into account the Galactic reddening of E(B-V)=0.024, the Swift/UVOT magnitudes correspond to a black-body emission with the temperature 27000 K (source frame). The high colour temperature suggest Gaia17dbg is unlikely to be a supernova and is rather an AGN flare or a TDE.

A new Swift/XRT observation of Gaia17dbg was obtained on 2018-06-08 (after the solar conjunction gap) resulted in a non-detection. However, when the three Swift/XRT data sets are combined together, the resulting 4.8 ks exposure image reveals a four-sigma (0.004 +/-0.001 cts/s) X-ray source at the position of the transient.

Swift/UVOT photometry in Table 4.2 shows the source remains bright in UV compared to the archival GALEX detection at NUV=21.1 +/-0.2. The X-ray detection and blue UV colours are consistent with both AGN and TDE explanations of the Gaia17dbg event.

JD	Band	MagAB	Err.
2458093.28	UVW2	19.13	0.06
2458093.31	UVM2	19.23	0.08
2458093.31	UVW1	19.12	0.07
2458093.07	UVW1	19.12	0.07
2458117.30	UVW1	18.91	0.07
2458278.14	UVW1	19.33	0.08
2458093.07	UVM2	19.23	0.08
2458117.30	UVM2	19.31	0.08
2458278.13	UVM2	19.42	0.09
2458093.07	UVW2	19.13	0.06
2458117.29	UVW2	19.04	0.06
2458278.13	UVW2	19.03	0.06

Table 4.2: Swift/UVOT photometry.

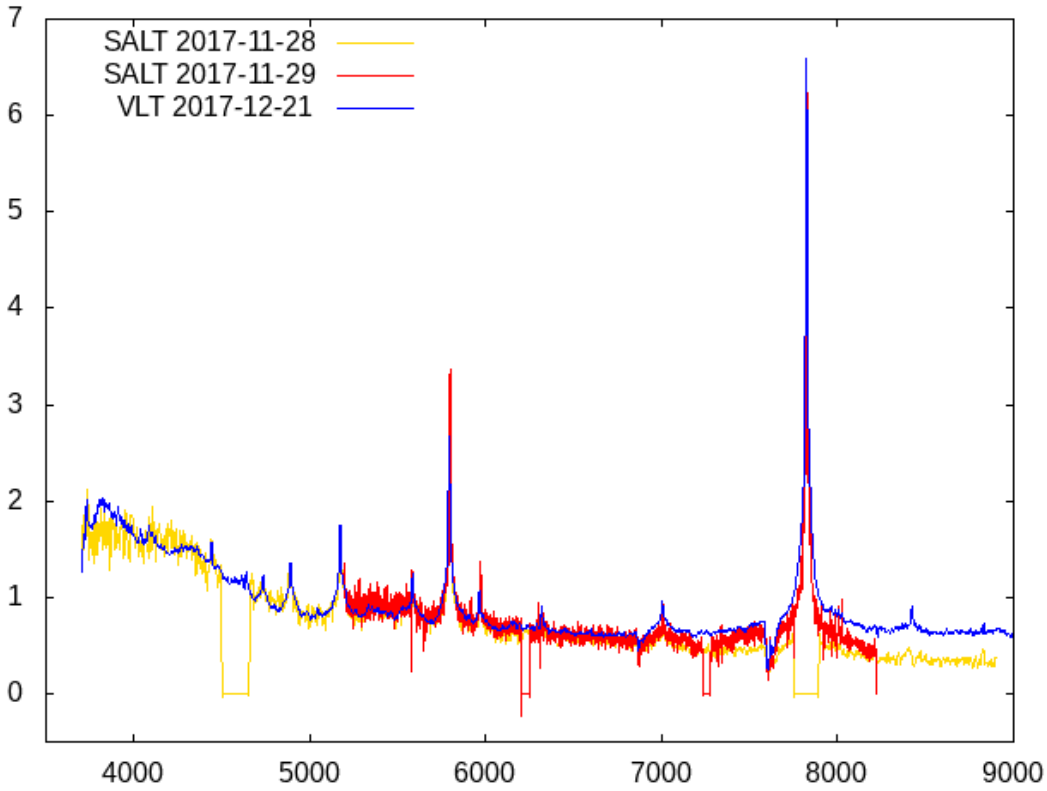

Figure 4.20: All obtained spectra for Gaia17dbg. The observed dates and telescopes are noted in the legend.

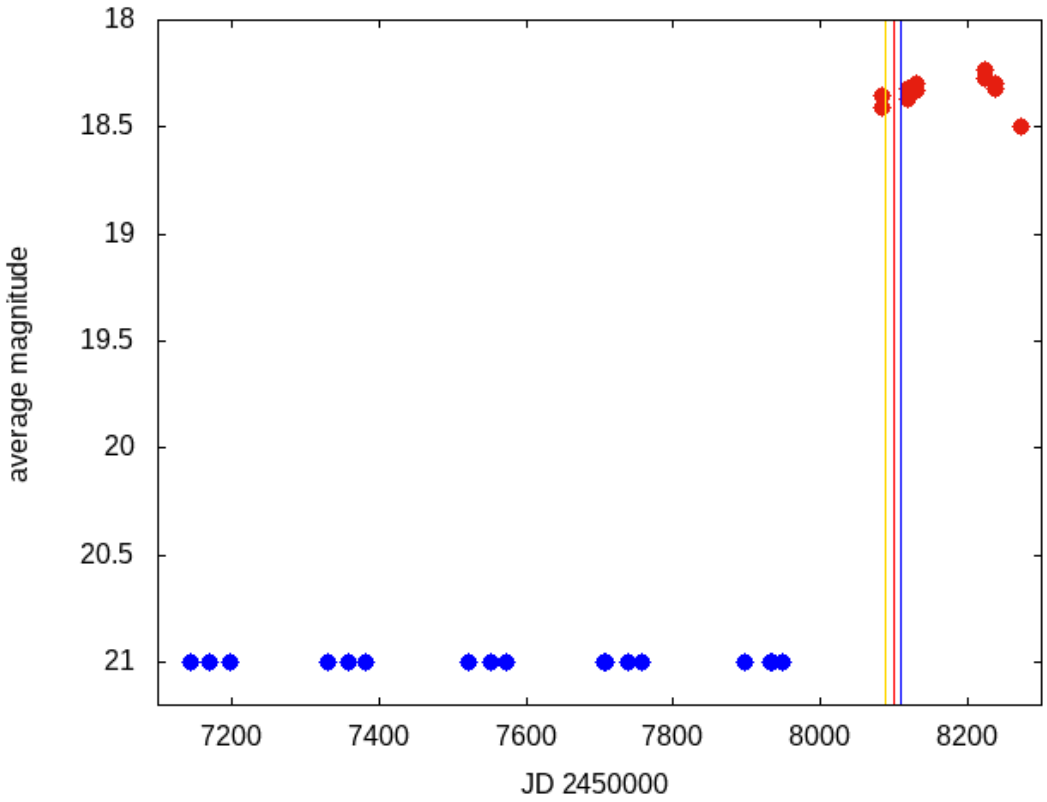

Figure 4.21: Lightcurve for Gaia17dbg shows part of the rising magnitude and after 100 days decreasing. The magnitudes are in Gaia's G-band. Red dots are detections and blue ones non-detections. Vertical lines represent times when spectra were taken, blue one marks time when spectrum from Figure 4.19 was taken, red one is for spectrum from Figure 4.18. All three spectra are plotted in Figure 4.20.

4.6 Gaia18aeo

The nuclear transient Gaia18aeo also known as AT2018ig was discovered by Gaia Science Alerts program on 2018-01-17. The transient was detected in the nucleus of the host galaxy LEDA 634652 at coordinates RA=03:06:37.26, dec=-36:37:05.92.

A low resolution (R = 350) SALT/RSS spectrum was taken on 2018-02-09.

The spectroscopic classification done using SNID code matched transient to SN Type Ia at about 3 weeks past maximum (Figure 4.22). However, additional classification done with DASH matched spectrum with SN IIb (Fifure 4.23), though the fit in DASH doesn't look convincing as it is not fitted properly and is fairly off as can be seen.

Spectrum shows narrow emission Hα line and also broad HeI present due to host galaxy and corresponds to redshift z=0.086±0.001. Gaia photometric measurement at the moment of observation (presumably after the peak but still near) and at this redshift corresponds to absolute magnitude of about -19.79 mag (without host subtraction), which is consistent with Type Ia.

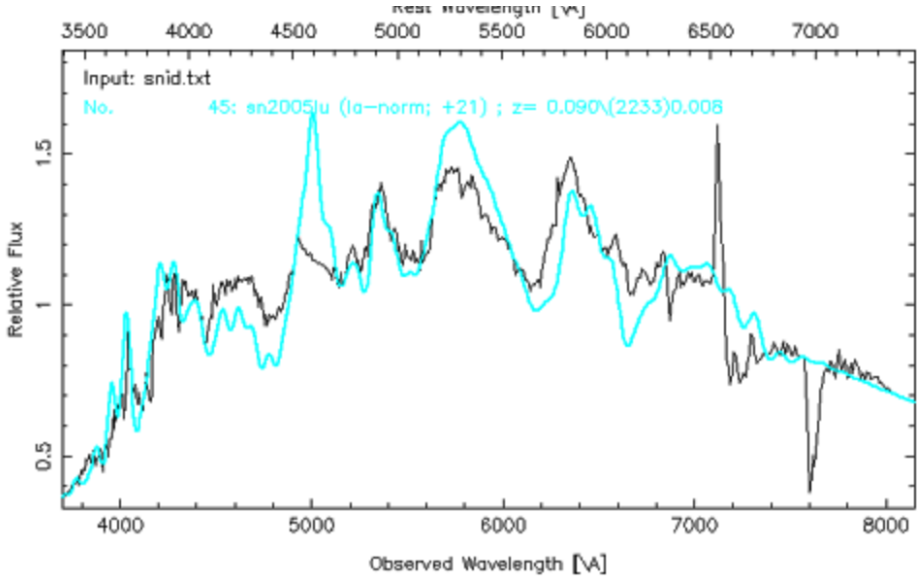

Figure 4.22: Spectroscopic classification of Gaia18aeo, using SNID code. It matched to SN Ia-norm, 31 days after the maximum.

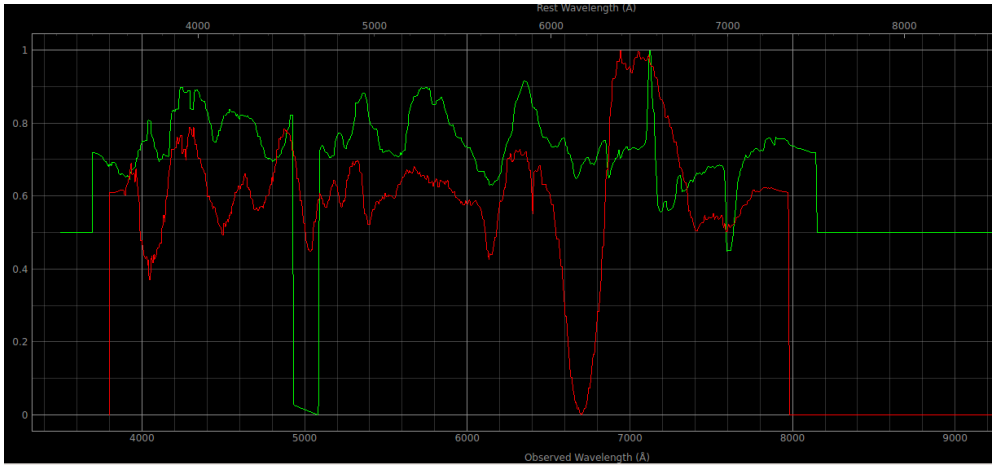

Figure 4.23: Spectroscopic classification of Gaia18aeo, using DASH code.

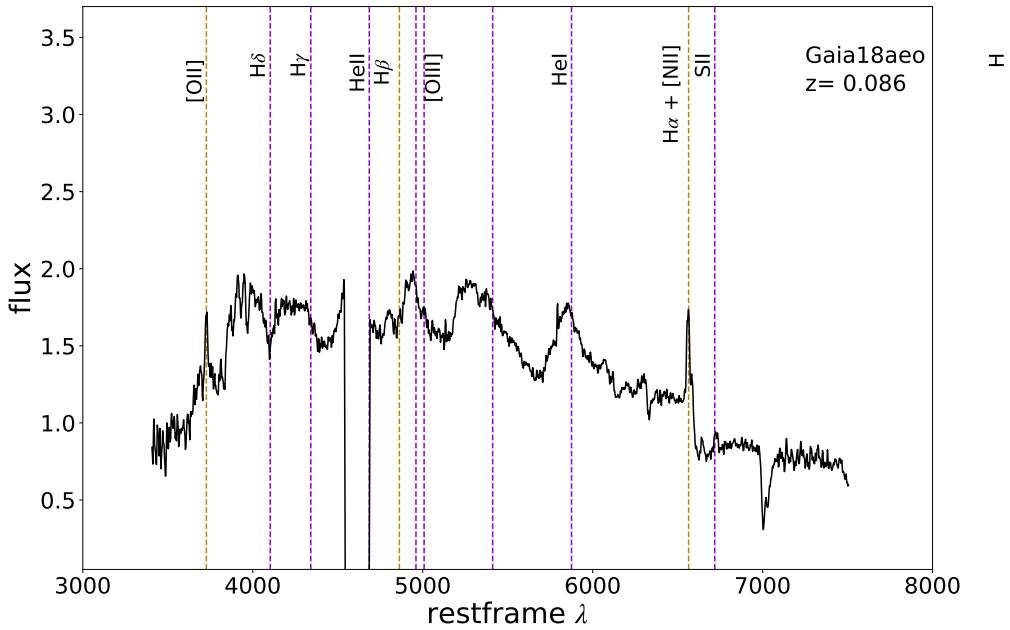

Figure 4.24: Spectrum of Gaia18aeo with marked spectral lines. Spectrum was taken with SALT on 2018-02-09.

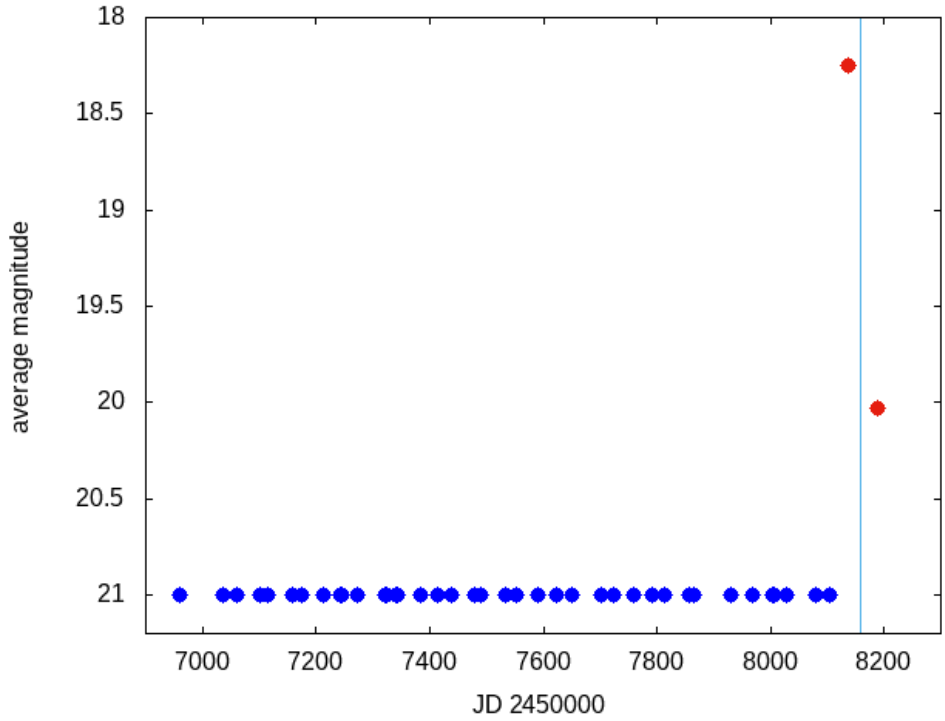

Figure 4.25: Lightcurve for Gaia18aeo. Data is detected with Gaia's *G-band*. Blue ones present non-detections and red ones detections, with vertical line marking time of taken spectrum. Unfortunately not much can be said about it, except that it is declining.

4.7 Gaia18aoq

The optical transient Gaia18aoq also known as AT2018aev was discovered by Gaia Science Alerts program on 2018-01-31. The transient was coinciding with the nucleus of galaxy 2MASX J13550786-3823227 on coordinates RA=13:55:07.91, dec=-38:23:22.74 . The alerting magnitude was 18.61.

The spectrum was obtained on 2018-03-14 with FORS2 on VLT.

The spectroscopic classification was originally done using SNID code and it was matched to SN Type IIP, 9 days past maximum as shown in Figure 4.26. Again, I checked classification with DASH and it also matched Gaia18aql to IIp (Figure 4.34). I estimated the redshift z=0.026±0.002 based on Hα which gives the absolute magnitude (just before the peak) of the transient of approximately -16.84 mag and without the subtracted galaxy. The spectrum shows blue continuum with superimposed emission lines of the Balmer series, [O II], [O III] and faint S II and H-beta .

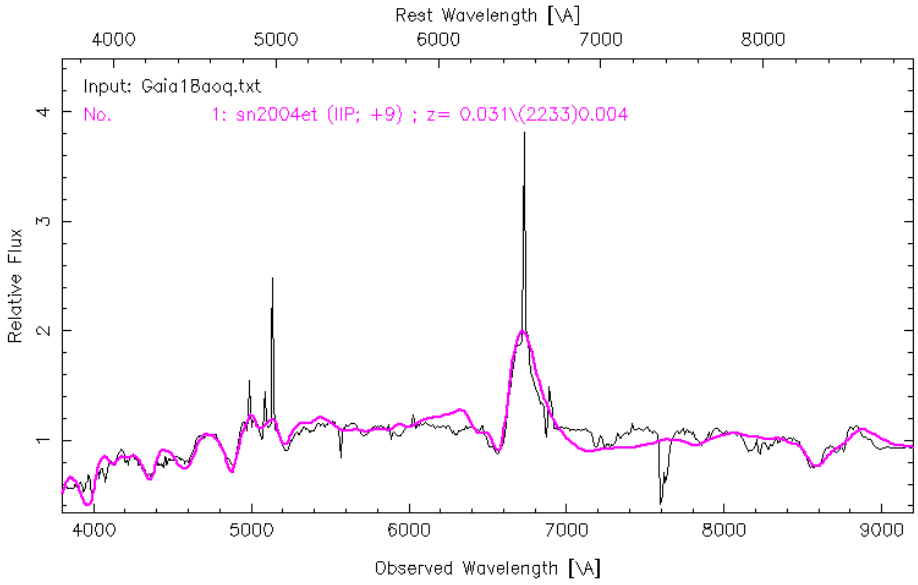

Figure 4.26: Spectroscopic classification of Gaia18aoq, using SNID code, matching it to SN IIp.

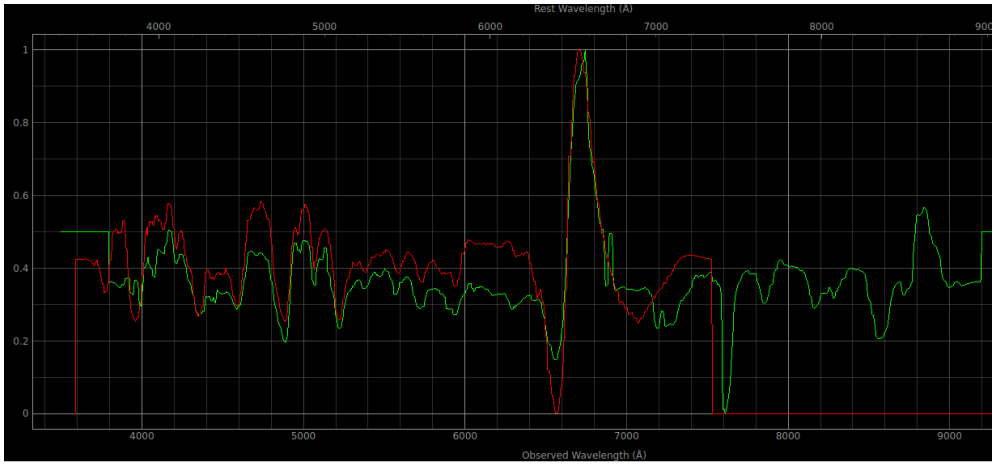

Figure 4.27: Spectroscopic classification of Gaia18aoq, using DASH code which also matched it to SN IIp.

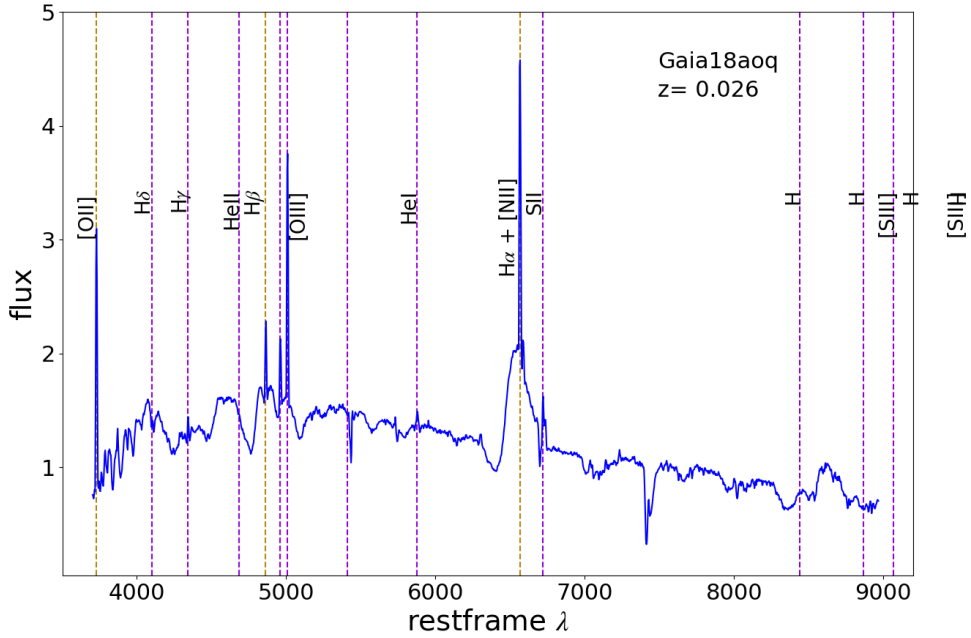

Figure 4.28: Spectrum of Gaia18aoq with marked spectral lines. Spectrum was taken with VLT on 2018-03-14.

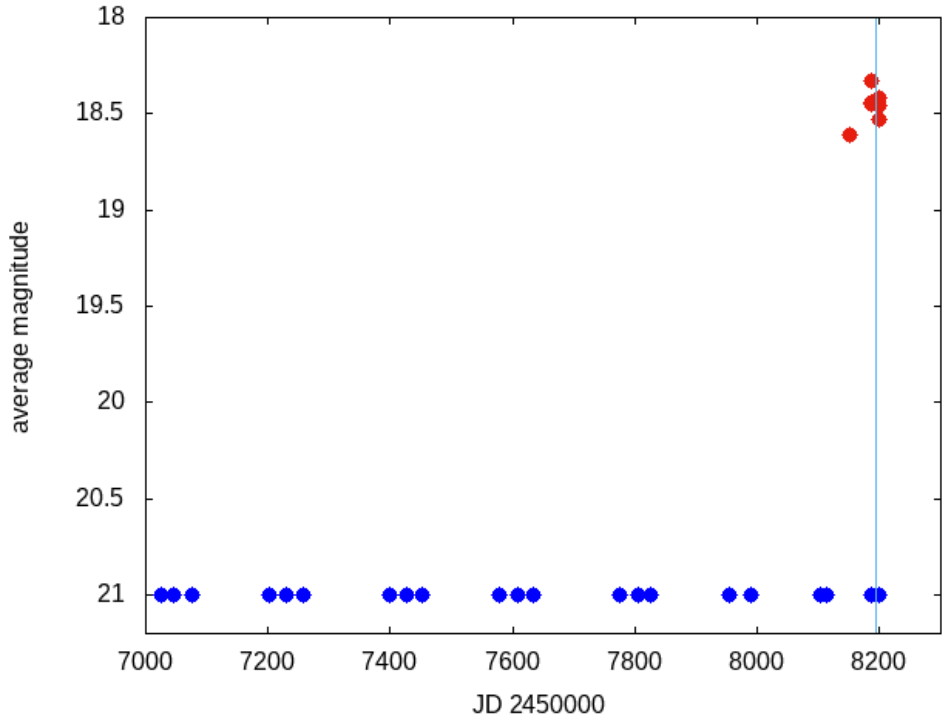

Figure 4.29: Lightcurve for Gaia18aoq shows the first detection (red dots) before the peak and then the next ones (after approximately a month) are already decreasing. It is unknown when was the peak. Blue dots represent non-detections. Vertical line marking time of taken spectrum from Figure 4.28.

4.8 OGLE18wc

The optical transient OGLE18wc also known as AT2018wc was detected on 2018-02-16 during the night of our dedicated search for fast transients CORTE (Chile-OGLE Rapid Transients Experiment) with the goal to get follow-up observation the same night as the detection is triggered. The flare lasted three days, reached about 19.1 mag in OGLE I-band at maximum (host subtracted, the light curve is shown in Figure 4.31) and coincided with the nucleus of a small galaxy at coordinates RA=05:18:11.72 and dec=-51:44:03.97.

The galaxy coincided with WISE J051811.72-514404.0, a candidate BL Lac type object[33] on the basis of its WISE colours and identification with the radio source SUMSS J051811-514404 (76.0 mJy at 843 MHz). The radio source is also detected with astrometric VLBI: ra 05:18:11.727160, dec -51:44:03.97925 +/-2.6 mas J2000 (30 mJy at 8.4 GHz). The X-ray source XMMSL2 J051811.6-514354 is located 10" away and, despite the reported 4.3" uncertainty in its position, is likely associated with the transient.

The spectrum of OGLE18wc was obtained on 2018-02-19 using the VLT/-FORS2 with grism 600V (3500-6300A). Additional low resolution spectra were obtained with SALT/RSS (3500-9200A) on 2018-02-20 and 2018-03-04. The spectra suggest rapid evolution as can be seen in Figure 4.30, but the difference between the VLT and SALT spectra can be also partly attributed to the slit alignment. The first (VLT) spectrum shown Hβ, Hg, [OIII] and [OII] emission lines and absorption lines of Ca II, G-band and Mg I at z=0.22. In the second (SALT) spectrum Hβ disappears, strong Iron complexes 4500Å and 5500Å are present. A broad Hα is visible having FWHM 4000km/s. The third (SALT) spectrum is similar to the second one but flux in red part has decreased by about 25% and was taken on 2018-03-20 (Figure 4.32).

Swift observed OGLE18wc for 2.0ks on 2018-02-21. The XRT detected an X-ray source with the net count rate of 0.013 +/-0.003 cts/s located 3.5" (error radius is 5.8") from the optical transient.

An UV source is detected at the position of the transient with the following UVOT Vega magnitudes:

Band	Mag.	Err.
UVW2	19.46	0.18
UVM2	19.74	0.29
UVW1	19.47	0.34
U	19.18	0.31
B	>19.86	
V	18.76	0.24

The above magnitudes are not corrected for the Galactic reddening of E(B-V)=0.013 and are not host-subtracted.

The Swift X-ray detection and blue UV colours together with the irregular lightcurve observed by OGLE-IV shown in Figure 4.31), WISE colors and archival VLBI detection suggest that OGLE18wc is a flaring blazar. The optical spectrum

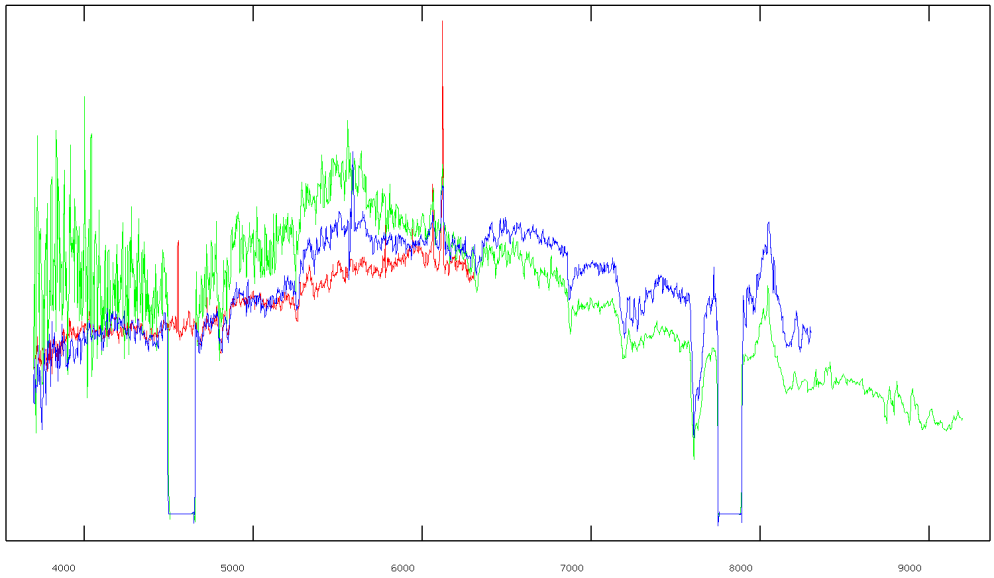

Figure 4.30: Spectra of OGLE18wc. Blue one one was taken on 2018-02-20 with SALT, the green one on 2018-03-04 with SALT and red one on 2018-02-19 with VLT.

of OGLE18wc resemble the spectrum of Mrk 501, a high-synchrotron peaked BL Lac type object that has a significant contribution from its host galaxy light in the optical band. OGLE18wc shows similarities to our spectrum of the Fermi-detected transient ASASSN-17gs/AT2017egv recently identified as a radio-weak BL Lac.

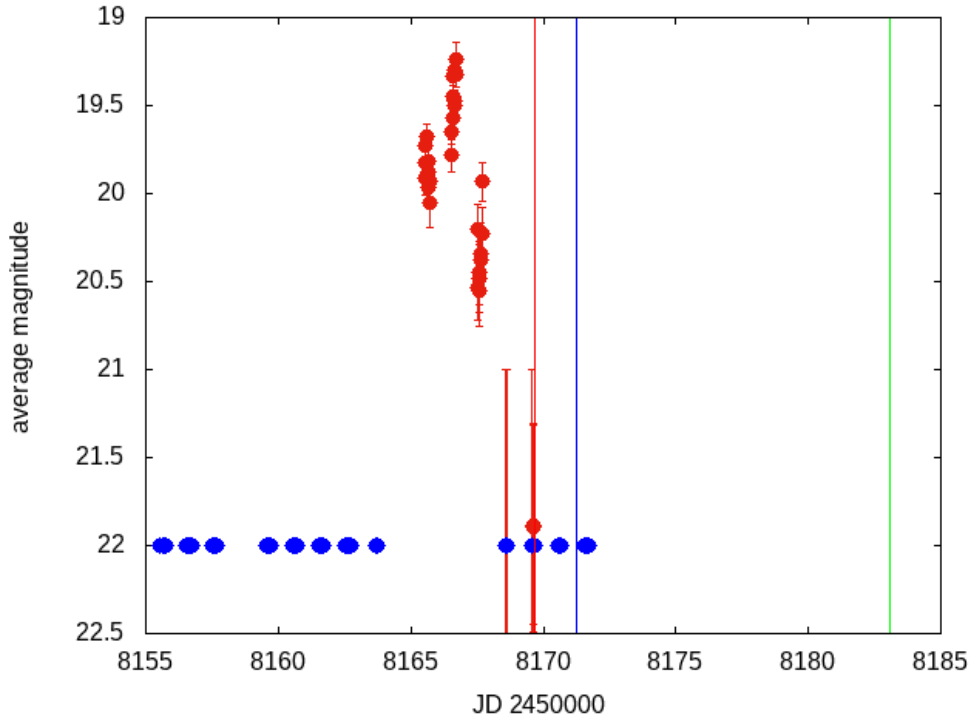

Figure 4.31: Irregular lightcurve for OGLE18wc, first looks like it is rising and after 10 days starts declining. All the data is taken with OBLE in *I-band*. Vertical lines represent times at which spectra were taken. The colours correspond to spectra in Figure 4.30

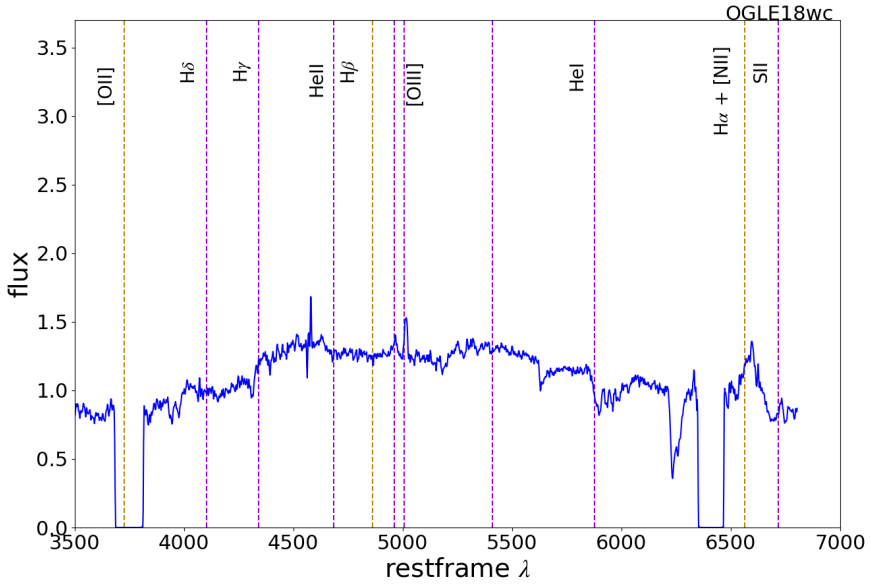

Figure 4.32: Spectrum of OGLE18wc with marked spectral lines taken on 2018-02-20 with SALT.

4.9 Gaia18aql

The optical transient Gaia18aql also known as AT2018zo and ATLAS18mgs was detected by Gaia Science Alerts program on 2018-03-15 in the nucleus of galaxy LEDA 57207 ar coordinates RA= 16:07:15.74 and dec=+26:11:48.05, with the previous detection by ATLAS. The alerting magnitude was 18.49.

The spectrum was obtained on 2018-03-20 with FORS2 on VLT. The spectroscopic classification was originally done using SNID code and it was matched to SN Type Ia, 21 days past maximum (Figure 4.33). Classification with DASH also matched spectrum wit one of SN Ia. Estimated redshift based on Hα line is z=0.054 which gives the absolute magnitude of the transient of approximately -18.49 mag.

The spectrum shows blue continuum with superimposed emission lines of the Balmer series, [O II], [O III] and S II normal for this SN type.

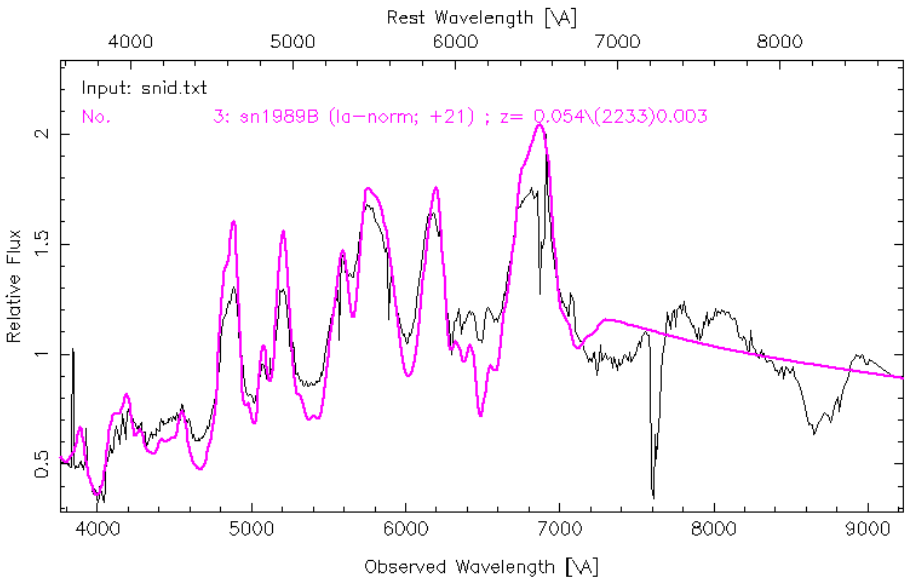

Figure 4.33: Spectroscopic classification of Gaia18aql, using SNID code. It was matched to SN Ia.

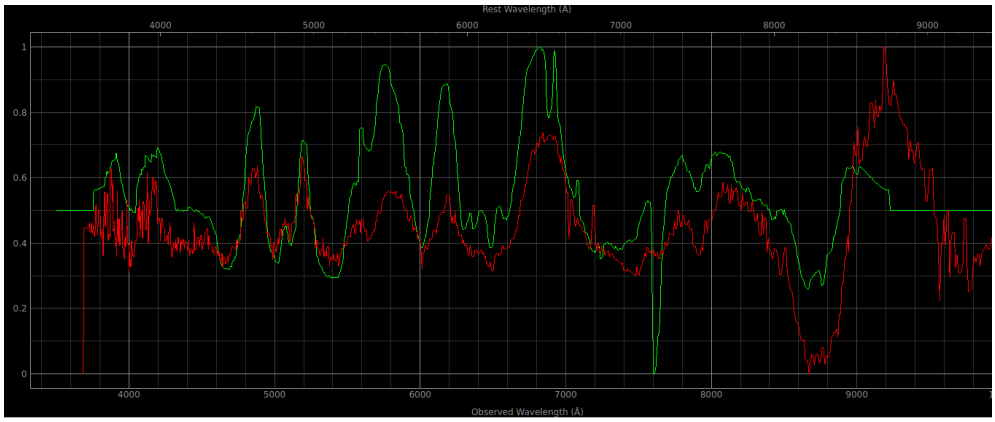

Figure 4.34: Spectroscopic classification of Gaia18aql, using DASH code. It was matched to SN Ia.

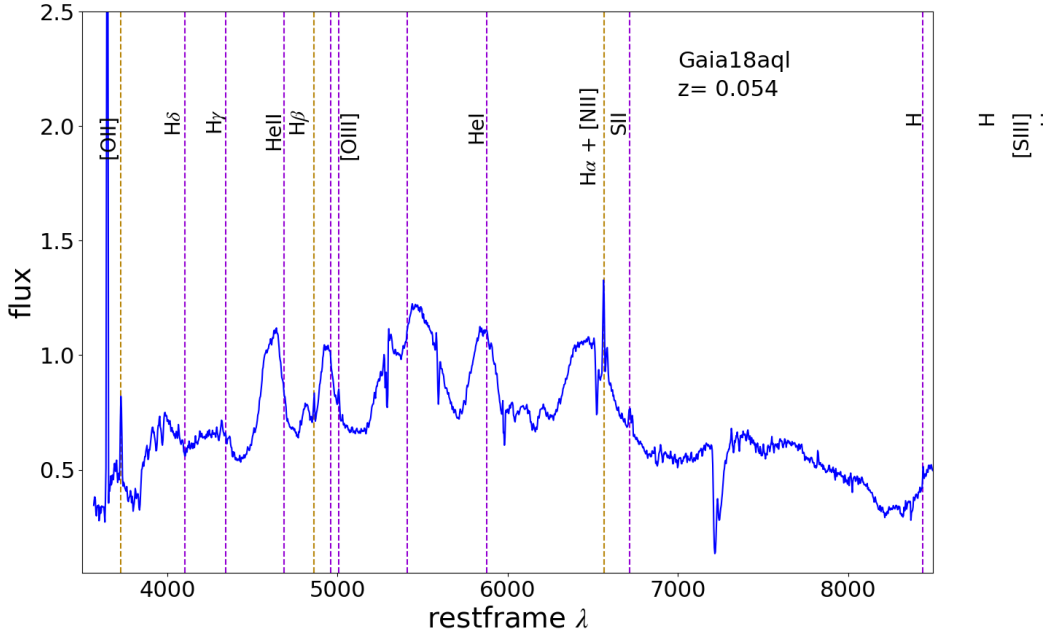

Figure 4.35: Spectrum of Gaia18aql with marked spectral lines taken with VLT on 2018-03-20.

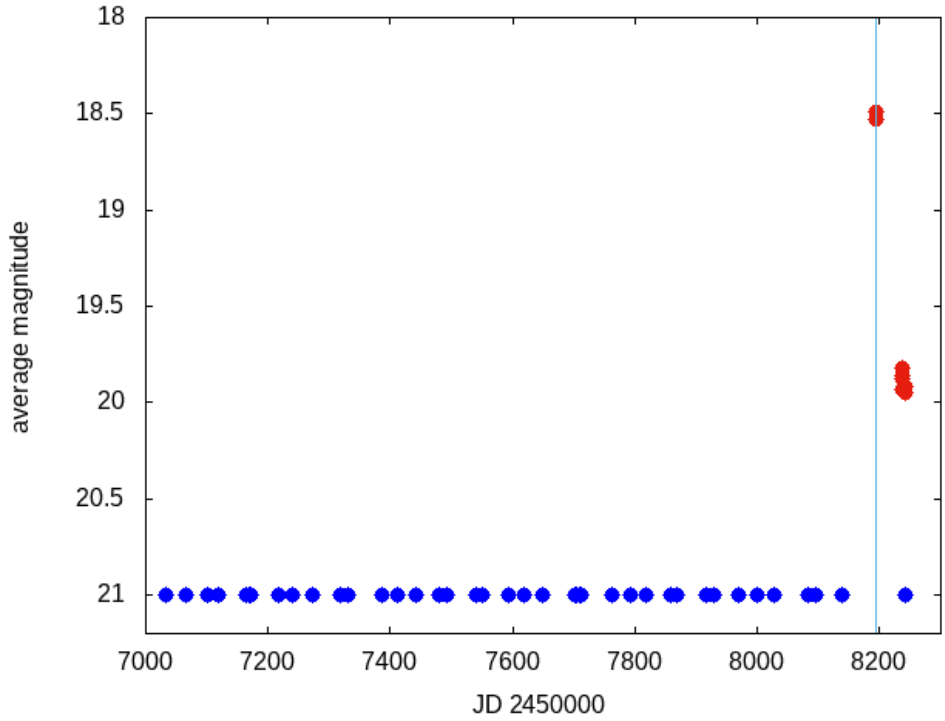

Figure 4.36: Lightcurve for Gaia18aql. The blue points represent non detections and the red ones detections from Gaia in G-bang. The vertical line shows time when spectrum was taken with VLT. The lightcurve shows that Gaia18aql is fading.

5 Conclusion

Technology advancements over the last two decades made a huge impact on astronomy. Not only that we can now look more precise and further in the Universe than we ever could, it also allowed huge development of wide field of view and all-sky survey satellites and ground based telescopes, detecting huge amount of new astronomical sources. This had huge importance on all fields of astronomy, especially on time domain astronomy, the study of how astronomical objects witch change with time.

There are two important necessities when studying changing astronomical objects - variable stars and transients - and this are large sky coverage with good cadence and precision. Two surveys match this description very well, i.e. ESA's satellite Gaia and Polish telescope OGLE.

In this work, I used data from both surveys. Gaia Photometric Science Alerts survey and OGLE-IV Transient Detection System both detect hundreds of new transients per day. I was interested in nuclear transients, especially rare events called Tidal Disruption Events (TDEs), phenomenon observed when a star gets too close to a Supermassive Black Hole (SMBH) in a centre of a galaxy and gets disrupted because of the gravitational pull of SMBH.

In the course of the work, there were around 40 candidates for nuclear transients detected with both surveys. Sixteen of them were not visible with any of the telescopes that we could use for the follow-up observations. Five of them were pre-classified (based on their spectra obtained with Gaia) to be supernovae type Ia and ten of them already had known redshift based on which I could determine absolute magnitude of the transient in question and eliminate them because they weren't bright enough to be TDEs or were already classified from previous detections. What was left were 9 candidates for which we obtained follow-up observations with VLT, SALT and Swift. Based on the classification of spectra from those 9 nuclear transients 4 of them turned out to be SN Ia, 2 of them SN IIp, 1 was a blazar, 1 what looked like flare from AGN and 1 TDE candidate. The last two are still being observed to further determine their nature.

Follow-up observations are crucial to determine the type of a transient. Further studies and observations are necessary, so that we will be able to investigate elusive TDEs and study the nature of quiescent black holes lurking in the centers of galaxies.

Bibliography

[1] D. Prialnik, *An Introduction to the Theory of Stellar Structure and Evolution*, Cambridge University Press (2010), Second edition.

[2] M.J. Rees *Tidal disruption of stars by black holes of* $10^6 - 10^8$ *solar masses in nearby galaxies*, Nature, Volume **333**, p523 (1988).

[3] Łukasz Wyrzykowski, M.Zieliński, et al. *OGLE16aaa- a Signature of a Hungry Super Massive Black Hole*, Monthly Notices of the Royal Astronomical Society: Letters, Volume **465**, Issue 1, p.L114-L118, arXiv:1606.03125

[4] C. S. Kochanek *Tidal Disruption Event (TDE) Demographics*, Monthly Notices of the Royal Astronomical Society, Volume **461**, Issue 1, p.371-384 arXiv:1601.06787

[5] Arcavi et al. *A continuum of H- to He- rich Tidal Disruption candidates with preference for E+A galaxies*, The Astrophysical Journal, Volume **793**, Issue 1, article id. 38, 16 pp. (2014), arXiv:1405.1415

[6] I. Arcavi, et al. *Core-collapse supernovae from the Palomar Transient Factory; Indications for a different population in dwarf galaxies*, The Astrophysical Journal, **721**, p 777-784, (2010)

[7] M. Mezcua *Observational evidence for intermediate-mass black holes* , International Journal of Modern Physics D, Volume **26**, Issue 11, id. 1730021 arXiv:1705.09667

[8] L.Eyer, B.Holl et al. *The Gaia Mission*, Astronomy & Astrophysics, Volume **595**, id.A1, 36 pp.

[9] Lukasz Wyrzykowski, Simon Hodgkin *Around Gaia Alerts in 20 questions* 2012, in Griffin E., Hanisch R., Seaman R., eds, IAU Symposium Vol. **285**, New Horizons in Time Domain Astronomy. pp 425-428

[10] N. Blagorodnova, et al. *GS-TEC: the Gaia Spectrophotometry Transient Events Classifier*, Monthly Notices of the Royal Astronomical Society, Volume **442**, Issue 1, p.327-342

[11] Opticon grant *http://www.astro-opticon.org/index.html* [cited: June 2018]

[12] Avishay Gal-Yam *Observational and Physical Classification of Supernovae*, Handbook of Supernovae, ISBN 978-3-319-21845-8. Springer International Publishing AG, 2017, p. 195

[13] Massimo Turatto *Classification of Supernovae*, Supernovae and Gamma-Ray Bursters. Edited by K. Weiler., Lecture Notes in Physics, vol. **598**, p.21-36, (2003).

[14] Main page of ESO's Very Large Telescope array, *http://www.eso.org/* [cited: May 2018]

[15] Main page of ESA's Gaia mission, *https://www.cosmos.esa.int/web/gaia/* [cited: May 2018]

[16] C. Jordi, M.Gebran, et al. *Gaia broad band photometry*, Astronomy and Astrophysics, Volume **523**, id.A48, 14 pp.(2010)

[17] A. Udalski, *The Optical Gravitational Lensing Experiment. Real Time Data Analysis Systems in the OGLE-III Survey*, Acta Astron.**53**:291,(2003).

[18] Main page of The Southern African Large Telescope *https://www.salt.ac.za/* [cited: May 2018]

[19] Main page of ESA *https://www.cosmos.esa.int/* [cited: May 2018]

[20] Main page of The Neil Gehrels Swift Observatory *https://swift.gsfc.nasa.gov/*/[cite August 2018]

[21] Cosmological Calculator for the Flat Universe http://home.fnal.gov/~gnedin/cc/ /[cite September 2017 - May 2018]

[22] M. Davis, J. Tonry *A survey of galaxy redshifts. I - Data reduction techniques*, Astronomical Journal, vol. **84**, p. 1511-1525, (1979).

[23] D. Muthukrishna, *DASH Documentation*, source code published on *https://astrodash.readthedocs.io/en/latest/index.html* [cited: January 2018 - August 2018]

[24] Jones, M., Lambourne, R. and Adams, D. (2004). *An Introduction to Galaxies and Cosmology.* Milton Keynes: Open University (2007)

[25] L. Wyrzykowski, Z. Kostrzewa-Rutkowska et al. *OGLE-IV Real-Time Transient Search* ACTA ASTRONOMICA Vol. **64**, pp. 197–232 (2014)

[26] A. Udalski, M.K.Szymański and G. Szymański *OGLE-IV: Fourth Phase of the Optical Gravitational Lensing Experiment* ACTA ASTRONOMICA Vol. **65** pp. 1–38, (2015)

[27] Astronomy *http://www.astronomy.com/magazine/2009/05/how-robots-are-looking-for-planets* [cited: August 2018]

[28] J. Magorrian, S. Tremaine, *Rates of tidal disruption of stars by massive central black holes*, MNRAS **309**, 9447 (1999).

[29] N. Blagorodnova, et al., *iPTF16fnl: A faint and fast tidal disruption event in an E+A galaxy*, The Astrophysical Joutnal Letters **844**, L21 (2016)

[30] E. M. Rossi, G. Lotado, *Multiband light curves of tidal disruption events*, MN-RAS **410**, p359 (2011).

[31] N. J. Secrest et al. *Identification of 1.4 million Active Galactic Nuclei in the mid-infrared using WISE data* The Astrophysical Journal Supplement Series, vol **221**, 12, (2015)

[32] Vanden Berk et al. *Composite Quasar Spectra from the Sloan Digital Sky Survey*, The Astronomical Journal, Volume **122**, Issue **2**, pp. 549-564. (2001).

[33] R. Abrusco et al. *The WISE blazar-like radio-loud sources: an all-sky catalog of candidate γ-ray blazars*, The Astrophysical Journal Supplement Series, Volume **215**, Number 1 (2014).

[34] Phinney E. S. *The Center of the Galaxy*, M. Morris (ed), IAU Symposium **136**, p543 (1989)

[35] Ihanec, N.; Gromadzki, M.; Wyrzykowski, L.; Buckley, D. A. H. *SALT spectroscopic classification of nuclear transients Gaia17cen/AT2017gld as SN Ia-91T* , The Astronomer's Telegram, No. 10738, (2017)

[36] Ihanec, N.; Gromadzki, M.; Wyrzykowski,L.; Iwanek, P.; Udalski, A. *VLT/FORS2 spectroscopic classification of nuclear transient OGLE17hil as normal Supernova Type Ia*, The Astronomer's Telegram, No. 10860, (2017)

[37] Sokolovsky, K.; Gromadzki, M.; Wyrzykowski,L. ; Ihanec, N., *Swift X-ray detection and VLT/FORS2 spectroscopy of the nuclear transient Gaia17cmd/AT2017har* , The Astronomer's Telegram, No. 10901, (2017)

[38] Ihanec, N.; Gromadzki, M.; Wyrzykowski, L.; Buckley, D. A. H. *SALT spectroscopic classification of nuclear transient Gaia17cqz/AT2017hrw as SN IIP* , The Astronomer's Telegram, No. 10943, (2017)

[39] Sokolovsky, K.; Gromadzki, M.; Wyrzykowski,L. ; Ihanec, N.; Soelen, B. Van; Buckley, D., *Swift and SALT observations the nuclear transient Gaia17dbg = ATLAS17lbg = AT2017gul* , The Astronomer's Telegram, No. 11049, (2017)

[40] Ihanec, N.; Gromadzki, M.; Wyrzykowski, L.; Buckley, D. A. H. *Classification of nuclear transient Gaia18aeo/AT2018ig as SN Ia with SALT spectroscopy* , The Astronomer's Telegram, No. 11291, (2018)

[41] Sokolovsky, K.; Gromadzki, M.; Wyrzykowski, L.; et al. *VLT, SALT and Swift observations confirm the blazar nature of OGLE18wc = AT2018wc* , The Astronomer's Telegram, No. 11434, (2018)

[42] Ihanec, N.; Gromadzki, M.; Wyrzykowski, L , *VLT/FORS2 spectroscopic classification of nuclear transient Gaia18aoq as Supernova Type IIP*, The Astronomer's Telegram, No. 11446, ,(2018)

[43] Ihanec, N.; Gromadzki, M.; Wyrzykowski, L, *VLT/FORS2 spectroscopic classification of nuclear transient Gaia18aql as Supernova Type Ia* , The Astronomer's Telegram, No. 11486, (2018)